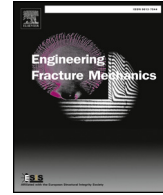




Contents lists available at ScienceDirect

Engineering Fracture Mechanics

journal homepage: www.elsevier.com/locate/engfracmech

Three-dimensional analytical model for effective elastic constants of transversely isotropic plates with multiple cracks: Application to stiffness reduction and steady-state cracking of composite laminates

Sota Onodera^{a,*}, Tomonaga Okabe^{a,b}^a Department of Aerospace Engineering, Tohoku University, 6-6-01 Aramaki-Aza-Aoba, Aoba-ku, Sendai 980-8579, Japan^b Department of Materials Science and Engineering, University of Washington, Seattle, WA 98195, USA

ARTICLE INFO

Keywords:

Fibre reinforced materials
 Polymer matrix composites
 Damage mechanics
 Micromechanics and/or materials
 Crack initiation

ABSTRACT

An analytical three-dimensional effective elastic constant of transversely isotropic plates that include ply cracks is proposed using a continuum damage mechanics approach. Two damage parameters associated with tensile and shear damage are formulated as functions of ply crack density using local stress fields that satisfy the equilibrium equations. Three-dimensional laminate theory is then employed to formulate the effective compliance of the laminate using the effective compliance of a damaged ply, and an analytical steady-state cracking model is established. The proposed model reproduces the thermomechanical properties and the crack initiation stress of laminates.

1. Introduction

In recent years, polymer matrix composites that have high specific strength and rigidity have been widely used in aerospace materials. Unidirectional fiber-reinforced polymer matrix composites are highly anisotropic; therefore, practical applications generally require various types of laminates made by stacking unidirectional fiber-reinforced ply, the fracture processes of which must be known to ensure safe design. The first form of damage in fiber-reinforced laminates is typically a ply crack [1], which grows to traverse the thickness of the ply and penetrate in the width direction parallel to the fibers in that ply. Although ply cracks are not critical to the final failure of composite laminates, these cracks significantly reduce the laminate's stiffness. The initiation of ply cracking results in stress concentration at the crack tip; therefore more severe damage, such as delamination and/or fiber breakage, occurs at the crack tip [2,3]. Hence, the thermomechanical properties of laminates that include ply cracks should be appropriately formulated to clarify the fracture mechanism of such laminates.

Several models for the stiffness reduction of laminates have been developed for cross-ply laminates [4,5], angle-ply laminates [6–8], and general symmetric laminates [9–11]. However, a model for general laminates should also be developed to clarify the fracture mechanism. Also, models for the stiffness reduction of laminates having arbitrary configurations have seldom been formulated.

Continuum damage mechanics (CDM) [12–17] is widely used to formulate the effective stiffness of a ply (or laminate) including ply cracks, and CDM has exhibited favorable compatibility with the laminate theory, which can address arbitrary configurations.

* Corresponding author.

E-mail address: sonodera@plum.mech.tohoku.ac.jp (S. Onodera).

<https://doi.org/10.1016/j.engfracmech.2019.106595>

Received 5 April 2019; Received in revised form 17 July 2019; Accepted 30 July 2019

Available online 07 August 2019

0013-7944/ © 2019 Elsevier Ltd. All rights reserved.

Nomenclature		λ_1, λ_2	material constants of the Laplace equation for displacement v
<i>Latin characters</i>		ν	Poisson's ratio
a, b	proportionality constants between $\varepsilon_x, \varepsilon_y,$ and ε_z	ξ	damage parameter related to shear loading
A	conversion matrix of stress and strain	ρ	ply crack density
C	stiffness matrix	ρ_N	normalized ply crack density
D_s	shear stiffness reduction	ρ_k^c	critical ply crack density
E	Young's modulus	σ	stress vector
$f(x, y), g(x, y)$	functions used in local stresses of damaged ply	$\bar{\sigma}$	stress vector divided into in-plane and out-of-plane parts
G	Shear modulus	$\bar{\sigma}^{\text{th}}$	stress to cancel out the thermal residual stress of the k -th ply
h	half of ply width	$\sigma^{L,\text{app}}$	uniaxial monotonic tensile stress of the laminate
l	half of crack spacing	$\sigma_c^{L,k}$	critical applied laminate stress when the cracks propagate in k -th ply
N	total number of plies	ω	damage parameter related to tensile loading
$P(i, j)$	elementary matrix that is interchanged in two rows (or two columns) i and j	<i>Sub/superscripts</i>	
R	coordinate conversion matrix of the strain	\bullet^0	related to undamaged property
S	compliance matrix	\bullet^1	related to damaged property
\bar{S}	compliance matrix for $\bar{\varepsilon}$ and $\bar{\sigma}$	$\bullet_1, \bullet_2, \bullet_3$	related to the longitudinal, in-plane, and out-of-plane transverse directions of ply
T	coordinate conversion matrix of the stress	$\bullet_{23}, \bullet_{31}, \bullet_{12}$	related to the 2–3, 3–1, and 1–2 plane
t	half of ply thickness	\bullet^{app}	related to applied ply stress or strain of ply in O-123
t_k	ply thickness of k -th ply	\bullet^{ave}	related to average ply stress or strain of ply in O-123
t_L	laminare thickness	\bullet^k	components of the k -th ply
T	testing temperature	\bullet^L	component of the laminate
T_{sf}	stress-free temperature	\bullet^{max}	related to maximum value
U	strain energy	\bullet_1, \bullet_0	related to in-plane parts and out-of-plane parts
u, v, w	displacements in the x -, y -, and z -directions	$\bullet_{11}, \bullet_{10}, \bullet_{00}$	3×3 compliance submatrix of the 6×6 compliance matrix
v_{COD}	crack opening displacement	$\bullet_x, \bullet_y, \bullet_z$	related to the 3-, 2-, and 1-directions
x, y, z	coordinate system of the representative volume element of damaged ply	$\bullet_{xy}, \bullet_{yz}, \bullet_{zx}$	related to the x - y , y - z , and z - x plane
X, Y, Z	coordinate system of the laminate	$\bullet_x, \bullet_y, \bullet_z$	related to the longitudinal, in-plane, and out-of-plane transverse directions of laminate
<i>Greek characters</i>		$\bullet_{XY}, \bullet_{YZ}, \bullet_{ZX}$	related to the X - Y , Y - Z , and Z - X plane
α	thermal expansion coefficient vector	<i>Abbreviations</i>	
$\bar{\alpha}$	thermal expansion coefficient vector divided into in-plane and out-of-plane parts	CDM	continuum damage mechanics
γ	engineering shear strain	CFRP	carbon fiber-reinforced plastic
Γ^k	energy release rate associated with ply crack of k -th ply	FEA	finite-element analysis
Γ^c	critical energy release rate	GFRP	glass fiber-reinforced plastic
Δ	material constant used in the stiffness matrix	LRAM	Large Radius Axisymmetric Damage Model
ΔT	temperature change	NPL	National Physical Laboratory
ε	strain vector		
$\bar{\varepsilon}$	strain vector divided into in-plane and out-of-plane parts		
θ^k	fiber angle of k -th ply between the 1- and X - axis		

Kachanov first proposed CDM [18]. Later, Allen et al. [12] and Talreja [16] applied CDM to fiber-reinforced composites. In CDM models, damage parameters are used to represent the extent of damage in a material. The damage parameters can be formulated using the average crack opening displacement based on linear fracture mechanics [19] or the local stress field model in a ply including ply cracks [14,15]. Okabe et al. [15] formulated a two-dimensional effective compliance matrix of laminates including ply cracks based on the damage tensor given by Murakami [13]. However, this compliance matrix is not symmetric, and does not allow all properties of a damaged laminate including out-of-plane properties to be determined. A three-dimensional effective compliance (or effective stiffness) matrix is absolutely essential for completely determining the thermoelastic properties of damaged laminate. Talreja [16] characterizes eight material constants in the three-dimensional effective stiffness matrix of transversely isotropic composite materials with ply cracks by formulating the Helmholtz free energy for isothermal small deformation and small damage based on vector damage variables. Li et al. [20] associated these material constants derived by Talreja with elastic constants of transversely isotropic materials and two damage parameters. They conducted a parametric study of crack geometry and distribution

in a finite element-based study to determine the sensitivity of the effective stiffness matrix of a unidirectional composite plate with an elliptical crack on the damage parameters; however, the formulation of these damage parameters was not explicitly derived. Therefore, this study will attempt to determine formulations of these damage parameters analytically to accomplish the formulation of a three-dimensional symmetric effective stiffness matrix of transversely isotropic material with ply cracks.

In this study, we developed a stiffness reduction model of transversely isotropic composite plates with ply cracks based on the CDM approach formulated by Li et al. The two damage parameters were formulated as a function of ply crack density using local stress field models that satisfy the equilibrium equations subjected to tensile loading normal to the fiber and in-plane shear loading. These two damage parameters are implemented into the effective stiffness matrix of ply derived by Li et al. The three-dimensional laminate theory is then employed to describe the stiffness reduction of composite laminate with arbitrary lay-up configurations and ply cracks, and we validated this stiffness reduction model by comparing its results to experiment results and results of finite-element analysis. Finally, the energy release rate associated with ply cracking is formulated using the effective compliance of composite laminates. An energy-based steady-state cracking model is proposed, and the steady-state cracking stress of cross-ply laminates is calculated for comparison with previous analytical models.

This paper is organized as follows. Section 2 presents the theoretical model proposed in this study. In Section 3, the present model is compared with experiments and previous models for stiffness reduction and steady-state cracking of composite laminates. Section 4 presents the conclusions of this study. Furthermore, to help readers derive the formulation more easily, the Appendix describes the coordinate conversion to the laminate coordinate system, the formulation of conversion matrix \mathbf{A} for the stress and strain used in the three-dimensional laminate theory, and the formulation of the three-dimensional laminate theory.

2. Theory

2.1. Three-dimensional effective stiffness matrix for a ply with ply cracks

Under the condition of small deformation and small damage, a stiffness matrix of unidirectional ply with multiple ply cracks was derived using a CDM-based model [20]. As indicated in Fig. 1, the 1-axis is the fiber direction, the 2-axis is the transverse direction, and the 3-axis is the thickness direction.

The ply crack planes are assumed to be parallel to the 1–3 plane, and these cracks penetrate in the fiber direction and the thickness direction. According to Li et al., the relationship between the applied average ply stress σ^{app} and the applied ply strain ε^{app} not considering the thermal residual strain in the damaged ply in Fig. 1 is

$$\sigma^{\text{app}} = \mathbf{C}\varepsilon^{\text{app}}, \quad (1)$$

where

$$\sigma^{\text{app}} = [\sigma_1^{\text{app}} \quad \sigma_2^{\text{app}} \quad \sigma_3^{\text{app}} \quad \sigma_{23}^{\text{app}} \quad \sigma_{13}^{\text{app}} \quad \sigma_{12}^{\text{app}}]^T, \quad (2)$$

$$\varepsilon^{\text{app}} = [\varepsilon_1^{\text{app}} \quad \varepsilon_2^{\text{app}} \quad \varepsilon_3^{\text{app}} \quad \gamma_{23}^{\text{app}} \quad \gamma_{13}^{\text{app}} \quad \gamma_{12}^{\text{app}}]^T, \quad (3)$$

and the stiffness matrix of damaged ply \mathbf{C} is the sum of the stiffness matrix \mathbf{C}^0 of undamaged ply and the damage-related stiffness matrix \mathbf{C}^1 , expressed as

$$\mathbf{C} = [C_{ij}] = \mathbf{C}^0 + \mathbf{C}^1, \quad (4)$$

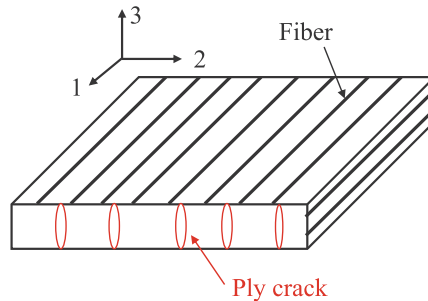


Fig. 1. Schematic of multiple ply cracks parallel to the fiber direction.

$$\mathbf{C}^0 = [C_{ij}^0] = \begin{bmatrix} \frac{1-\nu_{23}^0}{\Delta^0} E_1^0 & \frac{\nu_{12}^0}{\Delta^0} E_2^0 & \frac{\nu_{12}^0}{\Delta^0} E_2^0 & 0 & 0 & 0 \\ & \frac{1-\nu_{12}^0 \nu_{21}^0}{(1+\nu_{23}^0)\Delta^0} E_2^0 & \frac{\nu_{23}^0 + \nu_{12}^0 \nu_{21}^0}{(1+\nu_{23}^0)\Delta^0} E_2^0 & 0 & 0 & 0 \\ & & \frac{1-\nu_{12}^0 \nu_{21}^0}{(1+\nu_{23}^0)\Delta^0} E_2^0 & 0 & 0 & 0 \\ & & & G_{23}^0 & 0 & 0 \\ & & & & G_{12}^0 & 0 \\ \text{sym.} & & & & & G_{12}^0 \end{bmatrix}, \quad (5)$$

$$\mathbf{C}^1 = [C_{ij}^1] = -\omega \begin{bmatrix} \frac{E_1^0 \nu_{12}^0 \nu_{21}^0}{(\Delta^0)^2} & \frac{E_2^0 \nu_{12}^0 (1-\nu_{12}^0 \nu_{21}^0)}{(1+\nu_{23}^0)(\Delta^0)^2} & \frac{E_2^0 \nu_{12}^0 (\nu_{23}^0 + \nu_{12}^0 \nu_{21}^0)}{(1+\nu_{23}^0)(\Delta^0)^2} \\ & \frac{E_2^0 (1-\nu_{12}^0 \nu_{21}^0)^2}{(1+\nu_{23}^0)^2 (\Delta^0)^2} & \frac{E_2^0 (1-\nu_{12}^0 \nu_{21}^0) (\nu_{23}^0 + \nu_{12}^0 \nu_{21}^0)}{(1+\nu_{23}^0)^2 (\Delta^0)^2} \\ & & \frac{E_2^0 (\nu_{23}^0 + \nu_{12}^0 \nu_{21}^0)^2}{(1+\nu_{23}^0)^2 (\Delta^0)^2} \\ \text{sym.} & & & & & \\ & 0 & 0 & 0 \\ & 0 & 0 & 0 \\ & 0 & 0 & 0 \\ \frac{G_{23}^0}{2(1+\nu_{23}^0)} & 0 & 0 & \\ & 0 & 0 & \\ & & & \xi G_{12}^0 \end{bmatrix}, \quad (6)$$

where

$$\Delta^0 = 1 - \nu_{23}^0 - 2\nu_{12}^0 \nu_{21}^0, \quad (7)$$

$$\nu_{21}^0 = \frac{E_2^0}{E_1^0} \nu_{12}^0, \quad (8)$$

$$G_{23}^0 = \frac{E_2^0}{2(1+\nu_{23}^0)}. \quad (9)$$

Here, E is Young's modulus, G is the shear modulus, and ν is Poisson's ratio. The superscript 0 indicates the undamaged ply, and the subscripts indicate the coordinate axes of the ply. The parameter ω is associated with tensile damage, and ξ is associated with shear damage. These damage parameters are expressed as

$$\omega = 1 - \frac{E_2}{E_2^0}, \quad (10)$$

$$\xi = \frac{1}{\omega} \left(1 - \frac{G_{12}}{G_{12}^0} \right), \quad (11)$$

where E_2 is the Young's modulus of the damaged ply along the 2-axis, and G_{12} is the shear modulus of damaged ply in the 1–2 plane.

We formulate the damage parameters with the local stress field models using the proportion of the average ply strain, which ignores the crack opening displacement, to the applied ply strain considering crack opening displacement. When average stress σ_2^{app} is applied to the ply along the 2-axis, the average ply strain $\varepsilon_2^{\text{ave}}$ and the applied ply strain $\varepsilon_2^{\text{app}}$ along the 2-axis can be described as

$$\varepsilon_2^{\text{ave}} = \frac{\sigma_2^{\text{app}}}{E_2^0}, \quad (12)$$

$$\varepsilon_2^{\text{app}} = \frac{\sigma_2^{\text{app}}}{E_2}. \quad (13)$$

Using Eqs. (12) and (13), Eq. (10) is rewritten as

$$\omega = 1 - \frac{\varepsilon_2^{\text{ave}}}{\varepsilon_2^{\text{app}}}. \quad (14)$$

As for damage parameter ξ , which is a constant, when the ply is subjected to the shear stress σ_{12}^{app} in the 1–2 plane, the average ply engineering shear strain γ_{12}^{ave} and the applied ply engineering shear strain γ_{12}^{app} in the 1–2 plane are written as

$$\gamma_{12}^{\text{ave}} = \frac{\sigma_{12}^{\text{app}}}{G_{12}^0}, \quad (15)$$

$$\gamma_{12}^{\text{app}} = \frac{\sigma_{12}^{\text{app}}}{G_{12}}. \quad (16)$$

Using Eqs. (15) and (16), Eq. (11) can be reformulated as

$$\xi = \frac{1}{\omega} \left(1 - \frac{\gamma_{12}^{\text{ave}}}{\gamma_{12}^{\text{app}}} \right). \quad (17)$$

Eqs. (14) and (17) can be formulated as functions of ply crack density (i.e., the number of ply cracks per unit length normal to the crack plane) using the local stress field models for ply including cracks subjected to tensile loading along the 2-axis and shear loading in the 1–2 plane. The effective stiffness matrix \mathbf{C} is valid when damage parameter ω is very small (i.e., $\omega^2 \ll 1$). The maximum value of damage parameter ω when the model works effectively will be discussed in Section 3.1. The next subsection describes the formulation of the three-dimensional local stress field model with the damage parameters.

2.2. Damage parameters

A three-dimensional local stress field model of a ply that includes ply cracks was formulated to evaluate stiffness reduction. When formulating the local stress field model, the ply was assumed to be thin, and the damage was assumed to be caused mainly by ply cracks. Based on these assumptions, the damage due to delamination and fiber breakage were ignored.

A three-dimensional local stress field model is first formulated to subject the stress σ_2^{app} along the ply's 2-axis. Fig. 2 presents a representative volume element (RVE) that includes ply cracking on both sides of a part of the ply illustrated in Fig. 1.

The coordinate system in Fig. 2 differs from that in Fig. 1: the coordinates x , y , and z in Fig. 2 correspond to the 3-, 2-, and 1-axes in Fig. 1. The ply cracks are assumed to have tunnel-like crack surfaces that are symmetrical about the y -axis and are postulated not to propagate into the neighboring ply. The crack spacing is $2l$, the thickness of the ply is $t_k = 2t$, and the width of the ply is $2h$. The displacements in the x -, y -, and z -directions are defined as u , v , and w . The ply strain $\varepsilon_2^{\text{app}}$ along the y -axis (or 2-axis) is applied to the RVE (or ply). Because RVE is symmetric, the region of interest in this definition is limited to $0 \leq x \leq t$, $0 \leq y \leq l$, $0 \leq z \leq h$. The strain-stress relationship in the RVE is expressed as

$$\varepsilon_x = \frac{\partial u}{\partial x} = \frac{\sigma_x}{E_2^0} - \frac{\nu_{23}^0}{E_2^0} \sigma_y - \frac{\nu_{21}^0}{E_2^0} \sigma_z, \quad (18)$$

$$\varepsilon_y = \frac{\partial v}{\partial y} = -\frac{\nu_{23}^0}{E_2^0} \sigma_x + \frac{\sigma_y}{E_2^0} - \frac{\nu_{21}^0}{E_2^0} \sigma_z, \quad (19)$$

$$\varepsilon_z = \frac{\partial w}{\partial z} = -\frac{\nu_{21}^0}{E_2^0} \sigma_x - \frac{\nu_{21}^0}{E_2^0} \sigma_y + \frac{\sigma_z}{E_1^0}, \quad (20)$$

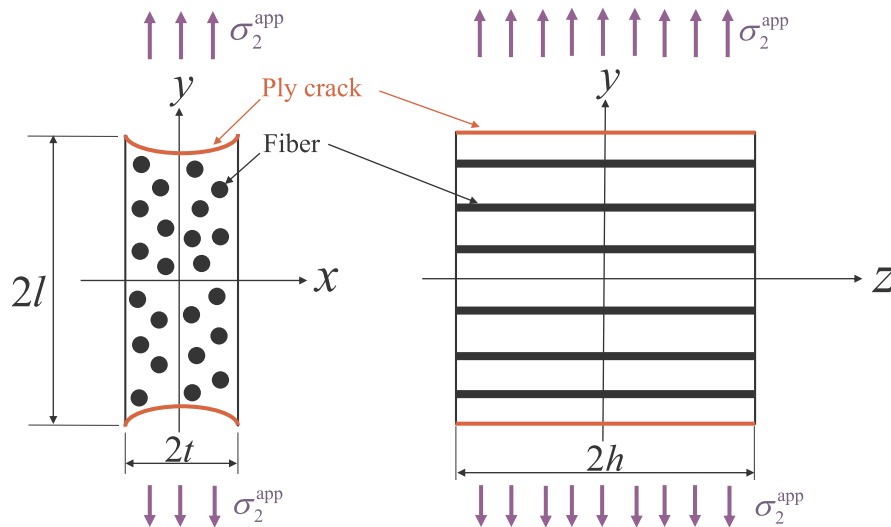


Fig. 2. Representative volume element subjected to tensile loading.

$$\gamma_{xy} = \frac{\sigma_{xy}}{G_{23}^0} = \frac{\partial v}{\partial x} + \frac{\partial u}{\partial y} \approx \frac{\partial v}{\partial x}, \quad (21)$$

$$\gamma_{yz} = \frac{\sigma_{yz}}{G_{12}^0} = \frac{\partial v}{\partial z} + \frac{\partial w}{\partial y} \approx \frac{\partial v}{\partial z}, \quad (22)$$

$$\gamma_{zx} = \frac{\sigma_{zx}}{G_{12}^0} = \frac{\partial u}{\partial z} + \frac{\partial w}{\partial x} \approx 0, \quad (23)$$

where σ_i ($i = x, y, z$) is the stress along the i -axis, ε_i is the strain along the i -axis, σ_{ij} ($j = x, y, z; j \neq i$) is the shear stress in the i - j plane, and γ_{ij} is the engineering shear strain in the i - j plane. For engineering shear strains γ_{xy} and γ_{yz} , the partial differential coefficients $\partial u/\partial y$ and $\partial w/\partial y$ are assumed to be quite small, and the engineering shear strain γ_{zx} is approximated as zero. Following Okabe et al. [15], the relationships between the strains ε_i are assumed as

$$\varepsilon_x = a\varepsilon_y, \quad (24)$$

$$\varepsilon_z = b\varepsilon_y, \quad (25)$$

where a and b are proportionality constants defined to satisfy the equilibrium equations of stress. The physical meaning of a and b is the average Poisson's ratio in the RVE. Using Eqs. (18)–(20), (24) and (25), σ_x , σ_y , and σ_z are expressed as

$$\sigma_x = E_2 \frac{\nu_{23}^0 + \nu_{12}^0 \nu_{21}^0 + (1 - \nu_{12}^0 \nu_{21}^0)a + \nu_{12}^0(1 + \nu_{23}^0)b}{(1 + \nu_{23}^0)(1 - \nu_{23}^0 - 2\nu_{12}^0 \nu_{21}^0)} \frac{\partial v}{\partial y}, \quad (26)$$

$$\sigma_y = E_2 \frac{1 - \nu_{12}^0 \nu_{21}^0 + (\nu_{23}^0 + \nu_{12}^0 \nu_{21}^0)a + \nu_{12}^0(1 + \nu_{23}^0)b}{(1 + \nu_{23}^0)(1 - \nu_{23}^0 - 2\nu_{12}^0 \nu_{21}^0)} \frac{\partial v}{\partial y}, \quad (27)$$

$$\sigma_z = E_1 \frac{\nu_{21}^0 + \nu_{21}^0 a + (1 - \nu_{23}^0)b}{1 - \nu_{23}^0 - 2\nu_{12}^0 \nu_{21}^0} \frac{\partial v}{\partial y}. \quad (28)$$

In addition, using Eqs. (21)–(23), the shear stresses σ_{xy} , σ_{yz} , and σ_{zx} are described as

$$\sigma_{xy} = G_{23}^0 \frac{\partial v}{\partial x}, \quad (29)$$

$$\sigma_{yz} = G_{12}^0 \frac{\partial v}{\partial z}, \quad (30)$$

$$\sigma_{zx} = 0. \quad (31)$$

The equilibrium equations of stress are expressed as

$$\frac{\partial \sigma_x}{\partial x} + \frac{\partial \sigma_{xy}}{\partial y} + \frac{\partial \sigma_{zx}}{\partial z} = 0, \quad (32)$$

$$\frac{\partial \sigma_{xy}}{\partial x} + \frac{\partial \sigma_y}{\partial y} + \frac{\partial \sigma_{yz}}{\partial z} = 0, \quad (33)$$

$$\frac{\partial \sigma_{zx}}{\partial x} + \frac{\partial \sigma_{yz}}{\partial y} + \frac{\partial \sigma_z}{\partial z} = 0. \quad (34)$$

Assuming that $\partial^2 v/\partial x \partial y \neq 0$ and $\partial^2 v/\partial y \partial z \neq 0$, and substituting Eqs. (26)–(31) into Eqs. (32)–(34), the proportionality constants a and b and the Laplace equation for displacement v are obtained as

$$a = - \left[\nu_{23}^0 + \frac{G_{23}^0}{E_2^0} \{1 - (\nu_{23}^0)^2\} - \frac{G_{12}^0}{E_1^0} \nu_{12}^0 (1 + \nu_{12}^0) \right], \quad (35)$$

$$b = - \left[\nu_{21}^0 - \frac{G_{23}^0}{E_2^0} \nu_{21}^0 (1 + \nu_{23}^0) + \frac{G_{12}^0}{E_1^0} (1 - \nu_{12}^0 \nu_{21}^0) \right], \quad (36)$$

$$\frac{\partial^2 v}{\partial x^2} + \lambda_1^2 \frac{\partial^2 v}{\partial y^2} + \lambda_2^2 \frac{\partial^2 v}{\partial z^2} = 0, \quad (37)$$

where constants λ_1 and λ_2 are defined as

$$\lambda_1 = \sqrt{\frac{E_2^0}{G_{23}^0} \frac{1 - \nu_{12}^0 \nu_{21}^0 + (\nu_{23}^0 + \nu_{12}^0 \nu_{21}^0)a + \nu_{12}^0(1 + \nu_{23}^0)b}{(1 + \nu_{23}^0)(1 - \nu_{23}^0 - 2\nu_{12}^0 \nu_{21}^0)}}, \quad (38)$$

$$\lambda_2 = \sqrt{\frac{G_{12}^0}{G_{23}^0}}. \quad (39)$$

To determine displacement v , the boundary conditions of the Laplace equation in Eq. (37) are given by

$$v = 0 \quad \text{on} \quad y = 0, \quad (40)$$

$$\frac{\partial v}{\partial y} = 0 \quad \text{on} \quad y = l, \quad (41)$$

$$\frac{\partial v}{\partial x} = 0 \quad \text{on} \quad x = 0, \quad (42)$$

$$\frac{\partial v}{\partial z} = 0 \quad \text{on} \quad z = h, \quad (43)$$

$$\frac{\partial v}{\partial z} = 0 \quad \text{on} \quad z = 0, \quad (44)$$

$$v = \varepsilon_2^{\text{app}} y \quad \text{on} \quad x = t. \quad (45)$$

At $y = 0$, no displacement v is considered in Eq. (40). Eq. (41) was determined from Eqs. (26)–(28) considering the stress condition $\sigma_x = \sigma_y = \sigma_z = 0$ at the crack surface ($y = l$). Eq. (42) was defined based on Eq. (29), considering the shear stress condition $\sigma_{xy} = 0$ on the center plane at $x = 0$ of the ply. Eq. (43) means that shear stress σ_{yz} expressed by Eq. (30) is zero on the surface at $z = h$, and Eq. (44) expresses that the shear stress σ_{yz} is zero on the center plane at $z = 0$ of the ply. In addition, the displacement distribution in the interface, presented as Eq. (45), is assumed based on the previous study [14]. Therefore, the neighboring ply is thought to be deformed uniformly by mechanical loading $\varepsilon_2^{\text{app}}$, regardless of the ply cracks. Separating variables and assigning the boundary conditions presented above to Eq. (37), the solution $v(x, y, z)$ of the Laplace equation that satisfies the boundary conditions can be expressed as

$$v(x, y, z) = \frac{8l}{\pi^2} \left(\sum_{n=1}^{\infty} \frac{(-1)^{n+1} \cosh[(2n-1)\pi\lambda_1 x/(2l)]}{(2n-1)^2 \cosh[(2n-1)\pi\lambda_1 t/(2l)]} \sin\left[\frac{2n-1}{2l}\pi y\right] \right) \varepsilon_2^{\text{app}}. \quad (46)$$

When Eq. (46) is substituted into Eqs. (26)–(31), the local stress distribution under tensile loading along the 2-axis in the RVE is derived as

$$\sigma_x(x, y, z) = \frac{4E_2^0 \nu_{23}^0 + \nu_{12}^0 \nu_{21}^0 + (1 - \nu_{12}^0 \nu_{21}^0)a + \nu_{12}^0(1 + \nu_{23}^0)b}{\pi(1 + \nu_{23}^0)(1 - \nu_{23}^0 - 2\nu_{12}^0 \nu_{21}^0)} f(x, y) \varepsilon_2^{\text{app}}, \quad (47)$$

$$\sigma_y(x, y, z) = \frac{4E_2^0(1 - \nu_{12}^0 \nu_{21}^0 + (\nu_{23}^0 + \nu_{12}^0 \nu_{21}^0)a + \nu_{12}^0(1 + \nu_{23}^0)b}{\pi(1 + \nu_{23}^0)(1 - \nu_{23}^0 - 2\nu_{12}^0 \nu_{21}^0)} f(x, y) \varepsilon_2^{\text{app}}, \quad (48)$$

$$\sigma_z(x, y, z) = \frac{4E_1^0 \nu_{21}^0 + \nu_{21}^0 a + (1 - \nu_{23}^0)b}{\pi(1 - \nu_{23}^0 - 2\nu_{12}^0 \nu_{21}^0)} f(x, y) \varepsilon_2^{\text{app}}, \quad (49)$$

$$\sigma_{xy}(x, y, z) = \frac{4}{\pi} G_{23}^0 \lambda_1 g(x, y) \varepsilon_2^{\text{app}}, \quad (50)$$

$$\sigma_{yz}(x, y, z) = 0, \quad (51)$$

$$\sigma_{zx}(x, y, z) = 0, \quad (52)$$

where

$$f(x, y) = \sum_{n=1}^{\infty} \frac{(-1)^{n+1} \cosh[(2n-1)\pi\lambda_1 x/(2l)]}{2n-1 \cosh[(2n-1)\pi\lambda_1 t/(2l)]} \cos\left[\frac{2n-1}{2l}\pi y\right], \quad (53)$$

$$g(x, y) = \sum_{n=1}^{\infty} \frac{(-1)^{n+1} \sinh[(2n-1)\pi\lambda_1 x/(2l)]}{2n-1 \cosh[(2n-1)\pi\lambda_1 t/(2l)]} \sin\left[\frac{2n-1}{2l}\pi y\right]. \quad (54)$$

Thus, the local stress distribution in a ply that includes ply cracking is formulated. As indicated in Eqs. (46)–(54), the displacement v and the local stress distribution in a ply are constant with respect to the z -axis, and the shear stresses σ_{yz} and σ_{zx} are always zero. When the boundary condition given in Eqs. (40)–(45) is utilized, this local stress field model is close to the generalized plane strain state. The compatibility condition for the strain is not satisfied because of the assumption used in Eqs. (24) and (25). For carbon fiber reinforced plastic (CFRP), the local stress field model almost satisfies the plane strain condition because a is much larger than b . However, a is the same order as b when considering glass fiber reinforced plastic (GFRP). Therefore, parameters a and b that are

average Poisson's ratio are needed for GFRP ply. Strictly, a and b are functions of x , y , and z . However a and b are approximated by constants that satisfy the equilibrium equation of stress in the present model. Therefore, the proposed stress distributions are analytical solutions, but not exact solutions. Damage parameter ω can be formulated using the three-dimensional stress field model under tensile loading along the 2-axis. The average ply strain $\varepsilon_2^{\text{ave}}$ is defined as

$$\varepsilon_2^{\text{ave}} = \frac{1}{lth} \int_0^h \left(\int_0^l v(x, l, z) dx \right) dz. \quad (55)$$

By substituting Eq. (46) into Eq. (55), $\varepsilon_2^{\text{ave}}/\varepsilon_2^{\text{app}}$ is derived as

$$\frac{\varepsilon_2^{\text{ave}}}{\varepsilon_2^{\text{app}}} = \frac{16}{\pi^3 \lambda_1 t_k} \sum_{n=1}^{\infty} \frac{1}{(2n-1)^3} \frac{\tanh[(2n-1)\pi \lambda_1 t_k \rho / 2]}{\rho}, \quad (56)$$

where $\rho = 1/(2l)$ is ply crack density, and the thickness of the ply is defined as $t_k = 2t$. Using the above equation, Eq. (14) is reformulated as a function of ply crack density.

$$\omega = 1 - \frac{16}{\pi^3 \lambda_1 t_k} \sum_{n=1}^{\infty} \frac{1}{(2n-1)^3} \frac{\tanh[(2n-1)\pi \lambda_1 t_k \rho / 2]}{\rho} \quad (57)$$

As illustrated in Fig. 3 (a), a crack with a semi-tunnel-like surface may occur at the laminate surface.

In a thin laminate, surface cracks seriously affect the laminate's mechanical properties. Fig. 3 (b) depicts an RVE of a ply that has semi-tunnel-like cracks on the surface. Here, the area delineated by $0 \leq x \leq 2t$, $0 \leq y \leq l$, and $0 \leq z \leq h$ should be considered, because the RVE in Fig. 3 (b) is symmetrical with respect to the z - x and x - y planes. The mechanical behavior of a ply with a surface crack is assumed to be equal to the mechanical behavior of a ply with a ply crack that has twice the length of a surface crack. Based on this assumption, the surface crack can be considered by replacing ply thickness t_k with a thickness of $2t_k$. Thus, damage parameter ω can be represented to consider the surface crack by replacing t_k in Eq. (57) with $2t_k$ as follows.

$$\omega = 1 - \frac{8}{\pi^3 \lambda_1 t_k} \sum_{n=1}^{\infty} \frac{1}{(2n-1)^3} \frac{\tanh[(2n-1)\pi \lambda_1 t_k \rho]}{\rho} \quad (58)$$

When the cracks in a ply are considered, Eq. (57) is appropriate; Eq. (58) is appropriate to consider a ply with a surface crack.

Next, damage parameter ξ is derived to consider the damage due to ply cracking parallel to the fiber by formulating the local stress distribution of a ply with ply cracking subjected to shear loading. Fig. 4 depicts an RVE that includes a ply crack on both sides, which is a part of the ply illustrated in Fig. 1.

The x -, y -, and z -coordinates in Fig. 4 correspond to the 3-, 2- and 1-axes in Fig. 1. The in-plane ply shear stress σ_{12}^{app} is applied to the corresponding ply. The crack distance is $2l$, and the ply crack is assumed to have a tunnel-like surface that is symmetrical about the y -axis. Because the model is symmetric, the range is limited to $0 \leq x \leq t$, $0 \leq y \leq l$, $0 \leq z \leq h$. The deformations are assumed as

$$u(x, y, z) = v(x, y, z) = 0, \quad (59)$$

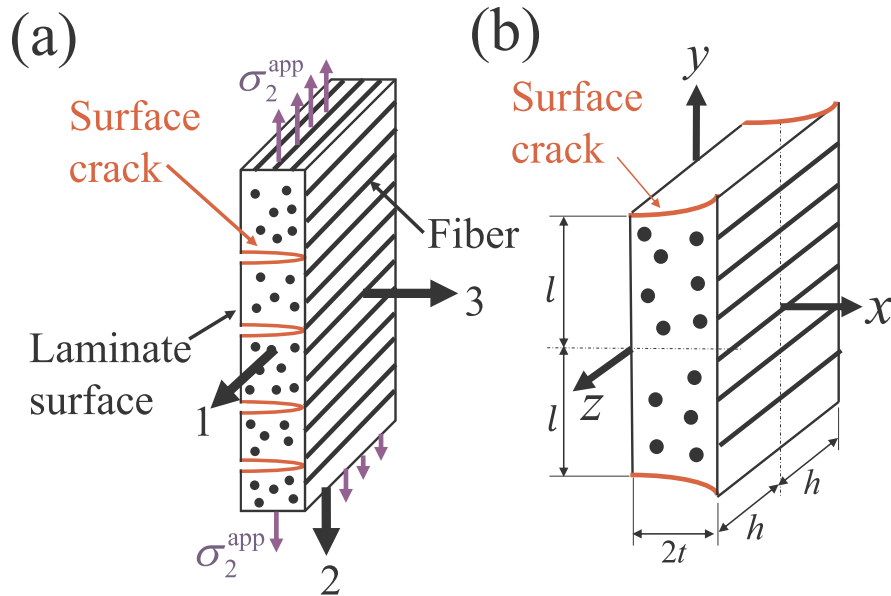


Fig. 3. (a) Ply including surface cracks. (b) Representative volume element.

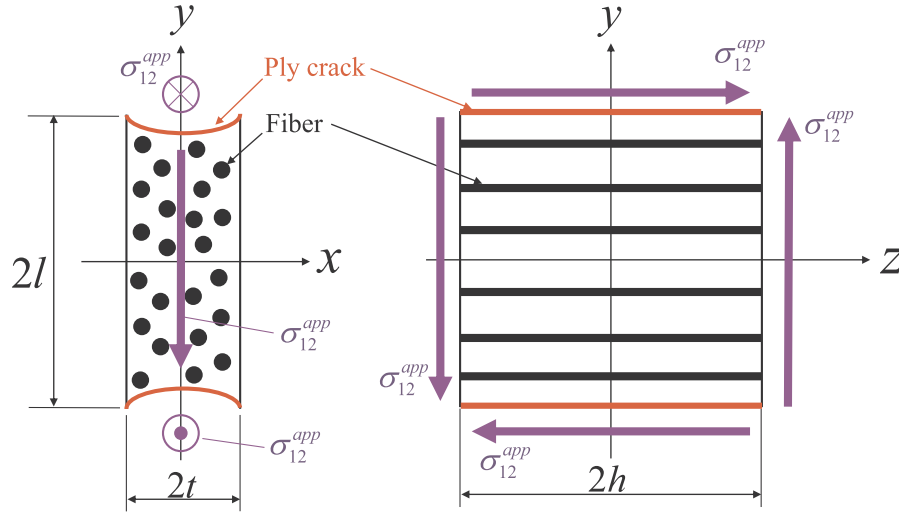


Fig. 4. Representative volume element subjected to shear loading.

$$w = w(x, y). \quad (60)$$

Under these assumptions, the strains of the cracked ply are expressed as

$$\varepsilon_x = \frac{\partial u}{\partial x} = \frac{\sigma_x}{E_2^0} - \frac{\nu_{23}^0}{E_2^0} \sigma_y - \frac{\nu_{21}^0}{E_2^0} \sigma_z = 0, \quad (61)$$

$$\varepsilon_y = \frac{\partial v}{\partial y} = -\frac{\nu_{23}^0}{E_2^0} \sigma_x + \frac{\sigma_y}{E_2^0} - \frac{\nu_{21}^0}{E_2^0} \sigma_z = 0, \quad (62)$$

$$\varepsilon_z = \frac{\partial w}{\partial z} = -\frac{\nu_{21}^0}{E_2^0} \sigma_x - \frac{\nu_{21}^0}{E_2^0} \sigma_y + \frac{\sigma_z}{E_1^0} = 0, \quad (63)$$

$$\gamma_{xy} = \frac{\sigma_{xy}}{G_{23}^0} = \frac{\partial v}{\partial x} + \frac{\partial u}{\partial y} = 0, \quad (64)$$

$$\gamma_{yz} = \frac{\sigma_{yz}}{G_{12}^0} = \frac{\partial v}{\partial z} + \frac{\partial w}{\partial y} = \frac{\partial w}{\partial y}, \quad (65)$$

$$\gamma_{zx} = \frac{\sigma_{zx}}{G_{12}^0} = \frac{\partial u}{\partial z} + \frac{\partial w}{\partial x} = \frac{\partial w}{\partial x}. \quad (66)$$

From Eqs. (59)–(66), the stresses of the cracked ply are expressed as

$$\sigma_x = \sigma_y = \sigma_z = \sigma_{xy} = 0, \quad (67)$$

$$\sigma_{yz} = G_{12}^0 \frac{\partial w}{\partial y} (x, y), \quad (68)$$

$$\sigma_{zx} = G_{12}^0 \frac{\partial w}{\partial x} (x, y). \quad (69)$$

When the stresses expressed by Eqs. (67)–(69) are substituted into equilibrium Eqs. (32)–(34), the Laplace equation for displacement w is obtained as

$$\frac{\partial^2 w}{\partial x^2} + \frac{\partial^2 w}{\partial y^2} = 0. \quad (70)$$

To determine the displacement w , the boundary conditions of Eq. (70) are given by

$$w = 0 \quad \text{on} \quad y = 0, \quad (71)$$

$$\frac{\partial w}{\partial y} = 0 \quad \text{on} \quad y = l, \quad (72)$$

$$\frac{\partial w}{\partial x} = 0 \quad \text{on } x = 0, \quad (73)$$

$$w = \gamma_{12}^{\text{app}} y \quad \text{on } x = t, \quad (74)$$

where γ_{12}^{app} is the applied ply shear strain. At $y = 0$, displacement w is not considered in Eq. (71). Eq. (72) is determined from Eq. (68), considering the shear stress condition $\sigma_{yz} = 0$ at the crack surface ($y = l$). Eq. (73) is defined based on Eq. (69) considering the shear stress condition $\sigma_{zx} = 0$ on the center plane ($x = 0$) of the ply. In addition, in the displacement distribution at the interface ($x = t$), presented as Eq. (74), the neighboring ply is assumed to deform uniformly by γ_{12}^{app} , regardless of the ply cracks. Separating variables and assigning the boundary conditions presented above to Eq. (70), the displacement $w(x, y)$ of the Laplace equation can be expressed as

$$w(x, y) = \frac{8l}{\pi^2} \sum_{n=1}^{\infty} \frac{(-1)^{n+1} \cosh[(2n-1)\pi x/(2l)]}{(2n-1)^2 \cosh[(2n-1)\pi t/(2l)]} \sin\left[\frac{2n-1}{2l}\pi y\right] \gamma_{12}^{\text{app}}. \quad (75)$$

When Eq. (75) is substituted into Eqs. (68) and (69), the local stress distribution under shear loading in the 1–2 plane in the RVE is derived as

$$\sigma_{yz} = \frac{4G_{12}^0}{\pi} \sum_{n=1}^{\infty} \frac{(-1)^{n+1} \cosh[(2n-1)\pi x/(2l)]}{2n-1 \cosh[(2n-1)\pi t/(2l)]} \cos\left[\frac{2n-1}{2l}\pi y\right] \gamma_{12}^{\text{app}}, \quad (76)$$

$$\sigma_{zx} = \frac{4G_{12}^0}{\pi} \sum_{n=1}^{\infty} \frac{(-1)^{n+1} \sinh[(2n-1)\pi x/(2l)]}{2n-1 \cosh[(2n-1)\pi t/(2l)]} \sin\left[\frac{2n-1}{2l}\pi y\right] \gamma_{12}^{\text{app}}. \quad (77)$$

Thus, the local stress distribution is formulated for a ply that includes ply cracking under shear loading. As indicated in Eq. (67) and Eqs. (75)–(77), displacement w and the local stress distribution in a ply are constant with respect to the z -axis. With shear loading, the compatibility condition for the strain is satisfied; therefore, the proposed stress distribution is an exact solution. Damage parameter ξ can be formulated using the three-dimensional stress field model for shear loading in the 1–2 plane. The average ply shear strain is defined as

$$\gamma_{12}^{\text{ave}} = \frac{1}{lth} \int_0^h \left(\int_0^t w(x, l) dx \right) dz. \quad (78)$$

By substituting Eq. (75) into Eq. (78), the proportion of the average ply shear strain to the applied ply shear strain is derived as

$$\frac{\gamma_{12}^{\text{ave}}}{\gamma_{12}^{\text{app}}} = \frac{16}{\pi^3 t_k} \sum_{n=1}^{\infty} \frac{1}{(2n-1)^3} \frac{\tanh[(2n-1)\pi t_k \rho / 2]}{\rho}. \quad (79)$$

Using Eq. (79), shear stiffness reduction $D_s(\rho)$ associated with ply cracking subjected to shear loading can be defined as [21]

$$D_s(\rho) \equiv 1 - \frac{\gamma_{12}^{\text{ave}}}{\gamma_{12}^{\text{app}}} = 1 - \frac{16}{\pi^3 t_k} \sum_{n=1}^{\infty} \frac{1}{(2n-1)^3} \frac{\tanh[(2n-1)\pi t_k \rho / 2]}{\rho}. \quad (80)$$

Under the condition of low crack density (or the range in which damage parameter ω is small), we found that the damage value D_s in Eq. (80) can be written with λ_1 given by Eq. (38) as

$$D_s = 1 - \frac{\gamma_{12}^{\text{ave}}}{\gamma_{12}^{\text{app}}} \approx \frac{1}{\lambda_1} \omega \quad (81)$$

Substituting Eq. (81) into Eq. (17), damage parameter ξ , which is a constant value, can be expressed using material parameter λ_1 .

$$\xi = \frac{1}{\lambda_1} \quad (82)$$

When considering the surface crack, damage parameter ξ is also written as Eq. (82). According to Li et al. [21], the constant shear damage parameter ξ depends on the material of ply and laminate lay-up configuration. Our derived shear damage parameter in Eq. (82) depends on the material of ply only because our local stress field model did not consider the stress transfer at the interface of the cracked ply.

When considering ply cracking, the effective stiffness matrix \mathbf{C} can be calculated using Eqs. (4), (57), and (82). The effective stiffness matrix \mathbf{C} for surface cracking can be calculated using Eqs. (4), (58), and (82). Because damage parameter ω is formulated as functions of ply crack density using the local stress field model, the stiffness matrix of the damaged ply is derived as a function of crack density. In the next subsection, the stiffness matrix of damaged ply was employed in the three-dimensional laminate theory to formulate the effective compliance and the effective thermal expansion coefficient of laminates with arbitrary configurations as a function of ply crack density.

2.3. Effective thermo-elastic properties of three-dimensional laminates with ply cracks

The effective thermo-elastic properties of three-dimensional laminates with ply cracks were formulated with the help of the three-dimensional laminate theory [19,22,23]. To determine the thermo-elastic properties of laminate utilizing the three-dimensional laminate theory, two-stage coordinate conversion is applied to the effective compliance and the thermal expansion coefficient of the k -th ply ($k = 1, 2, \dots, N; N$ is the total number of plies in the laminate) in the laminate. First, the compliance and the thermal expansion coefficient of the ply in principal axis O -123 is converted into those of the k -th ply in the coordinate system of laminate O -XYZ. We assume that the X - Y plane is parallel to the 1-2 plane of the ply and the Z -axis is in the same direction as the 3-axis. The direction of a fiber is tilted at an angle θ^k between the 1- and X -axes, as indicated in Fig. 5.

The constitutive law of the k -th ply in the laminate coordinate system O -XYZ is described as

$$\varepsilon^k = \mathbf{S}^k \sigma^k + \alpha^k \Delta T, \quad (83)$$

where ΔT is the temperature change $T - T_f$ from the stress-free temperature T_f to the testing temperature T . The effective compliance \mathbf{S}^k and the thermal expansion coefficient α^k of the k -th ply with cracks in the laminate coordinate system O -XYZ are formulated as (see Eqs. (106) and (108))

$$\mathbf{S}^k = \mathbf{R}^k(\theta^k) \mathbf{C}^{-1} \mathbf{T}^k(-\theta^k), \quad (84)$$

$$\alpha^k = \mathbf{R}^k(\theta^k) \alpha^0, \quad (85)$$

where superscript k denotes the components of the k -th ply, and the thermal expansion coefficient α^0 of a ply in the coordinate system of the principal axis of ply O -123 is defined as

$$\alpha^0 = [\alpha_1^0 \ \alpha_2^0 \ \alpha_3^0 \ 0 \ 0 \ 0]^T. \quad (86)$$

Here, α_1^0 is the thermal expansion coefficient of an undamaged ply along the 1-axis, and α_2^0 is that along the 2-axis. $\mathbf{T}^k(\theta^k)$ and $\mathbf{R}^k(\theta^k)$ are the coordinate conversion matrices of the stress and strain indicated in Eqs. (A.4) and (A.5). \mathbf{S}^k is calculated by substituting Eqs. (4), (A.4), and (A.5) into Eq. (84). Second, the stress, strain, and thermal expansion coefficient of the k -th ply are converted into those that are divided into in-plane parts and out-of-plane parts. The components of stress σ^k , strain ε^k , and thermal expansion coefficient α^k in the constitutive law of the k -th ply in Eq. (83) are defined as

$$\sigma^k = [\sigma_X^k \ \sigma_Y^k \ \sigma_Z^k \ \sigma_{YZ}^k \ \sigma_{ZX}^k \ \sigma_{XY}^k]^T, \quad (87)$$

$$\varepsilon^k = [\varepsilon_X^k \ \varepsilon_Y^k \ \varepsilon_Z^k \ \gamma_{YZ}^k \ \gamma_{ZX}^k \ \gamma_{XY}^k]^T, \quad (88)$$

$$\alpha^k = [\alpha_X^k \ \alpha_Y^k \ \alpha_Z^k \ 0 \ 0 \ 2\alpha_{XY}^k]^T. \quad (89)$$

The constitutive law of the stress $\bar{\sigma}^k$ and strain $\bar{\varepsilon}^k$ of the k -th ply that are divided into in-plane parts and out-of-plane parts can be described as

$$\bar{\varepsilon}^k = \bar{\mathbf{S}}^k \bar{\sigma}^k + \bar{\alpha}^k \Delta T, \quad (90)$$

where

$$\bar{\sigma}^k = \begin{bmatrix} \bar{\sigma}_1^k \\ \bar{\sigma}_0^k \end{bmatrix}, \quad \bar{\varepsilon}^k = \begin{bmatrix} \bar{\varepsilon}_1^k \\ \bar{\varepsilon}_0^k \end{bmatrix}, \quad \bar{\alpha}^k = \begin{bmatrix} \bar{\alpha}_1^k \\ \bar{\alpha}_0^k \end{bmatrix}, \quad (91)$$

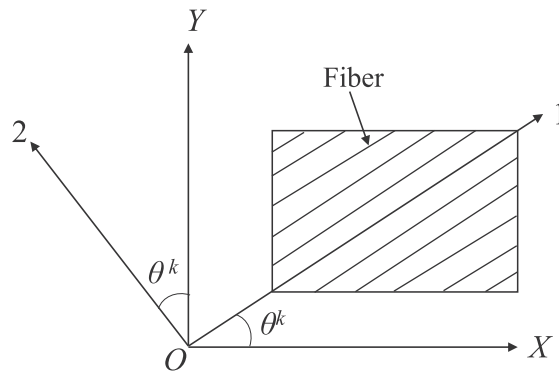


Fig. 5. In-plane coordinate conversion to the laminate coordinate system O -XYZ.

$$\bar{\sigma}_I^k = \begin{bmatrix} \sigma_X^k \\ \sigma_Y^k \\ \sigma_{XY}^k \end{bmatrix}, \quad \bar{\varepsilon}_I^k = \begin{bmatrix} \varepsilon_X^k \\ \varepsilon_Y^k \\ \gamma_{XY}^k \end{bmatrix}, \quad \bar{\alpha}_I^k = \begin{bmatrix} \alpha_X^k \\ \alpha_Y^k \\ 2\alpha_{XY}^k \end{bmatrix}, \quad (92)$$

$$\bar{\sigma}_O^k = \begin{bmatrix} \sigma_Z^k \\ \sigma_{ZX}^k \\ \sigma_{YZ}^k \end{bmatrix}, \quad \bar{\varepsilon}_O^k = \begin{bmatrix} \varepsilon_Z^k \\ \gamma_{ZX}^k \\ \gamma_{YZ}^k \end{bmatrix}, \quad \bar{\alpha}_O^k = \begin{bmatrix} \alpha_Z^k \\ 2\alpha_{ZX}^k \\ 2\alpha_{YZ}^k \end{bmatrix}. \quad (93)$$

Here, subscript I denotes the in-plane component, and O denotes the out-of-plane component. The relationship between Eqs. (87) and (88) and Eq. (91) can be formulated as

$$\bar{\sigma}^k = \mathbf{A}\sigma^k, \quad (94)$$

$$\bar{\varepsilon}^k = \mathbf{A}\varepsilon^k, \quad (95)$$

where \mathbf{A} is the conversion matrix in Eq. (B.3) (see Appendix B). Substituting Eqs. (94) and (95) into Eq. (83), the effective compliance and thermal expansion coefficient for the constitutive law between the strain and stress in Eq. (90) can be expressed using conversion matrix \mathbf{A} .

$$\bar{\mathbf{S}}^k = \begin{bmatrix} \bar{\mathbf{S}}_{II}^k & \bar{\mathbf{S}}_{IO}^k \\ (\bar{\mathbf{S}}_{IO}^k)^T & \bar{\mathbf{S}}_{OO}^k \end{bmatrix} = \mathbf{A}\mathbf{S}^k\mathbf{A}^T \quad (96)$$

$$\bar{\alpha}^k = \begin{bmatrix} \bar{\alpha}_I^k \\ \bar{\alpha}_O^k \end{bmatrix} = \mathbf{A}\alpha^k \quad (97)$$

Finally, using the three-dimensional laminate theory (see Appendix C), the constitutive law of laminate with arbitrary lay-ups is formulated as

$$\bar{\varepsilon}^L = \begin{bmatrix} \bar{\varepsilon}_I^L \\ \bar{\varepsilon}_O^L \end{bmatrix} = \bar{\mathbf{S}}^L\bar{\sigma}^L + \bar{\alpha}^L\Delta T = \begin{bmatrix} \bar{\mathbf{S}}_{II}^L & \bar{\mathbf{S}}_{IO}^L \\ (\bar{\mathbf{S}}_{IO}^L)^T & \bar{\mathbf{S}}_{OO}^L \end{bmatrix} \begin{bmatrix} \bar{\sigma}_I^L \\ \bar{\sigma}_O^L \end{bmatrix} + \begin{bmatrix} \bar{\alpha}_I^L \\ \bar{\alpha}_O^L \end{bmatrix} \Delta T, \quad (98)$$

where the stress and strain components are defined as

$$\bar{\sigma}^L = \begin{bmatrix} \bar{\sigma}_I^L \\ \bar{\sigma}_O^L \end{bmatrix}, \quad \bar{\varepsilon}^L = \begin{bmatrix} \bar{\varepsilon}_I^L \\ \bar{\varepsilon}_O^L \end{bmatrix}, \quad \bar{\alpha}^L = \begin{bmatrix} \bar{\alpha}_I^L \\ \bar{\alpha}_O^L \end{bmatrix}, \quad (99)$$

$$\bar{\sigma}_I^L = \begin{bmatrix} \sigma_X^L \\ \sigma_Y^L \\ \sigma_{XY}^L \end{bmatrix}, \quad \bar{\varepsilon}_I^L = \begin{bmatrix} \varepsilon_X^L \\ \varepsilon_Y^L \\ \gamma_{XY}^L \end{bmatrix}, \quad \bar{\alpha}_I^L = \begin{bmatrix} \alpha_X^L \\ \alpha_Y^L \\ 2\alpha_{XY}^L \end{bmatrix}, \quad (100)$$

$$\bar{\sigma}_O^L = \begin{bmatrix} \sigma_Z^L \\ \sigma_{ZX}^L \\ \sigma_{YZ}^L \end{bmatrix}, \quad \bar{\varepsilon}_O^L = \begin{bmatrix} \varepsilon_Z^L \\ \gamma_{ZX}^L \\ \gamma_{YZ}^L \end{bmatrix}, \quad \bar{\alpha}_O^L = \begin{bmatrix} \alpha_Z^L \\ 2\alpha_{ZX}^L \\ 2\alpha_{YZ}^L \end{bmatrix}, \quad (101)$$

and the effective compliance $\bar{\mathbf{S}}^L$ and effective thermal expansion coefficient $\bar{\alpha}^L$ of laminate with arbitrary lay-ups can be obtained as follows.

$$\bar{\mathbf{S}}^L = [\bar{S}_{ij}^L] = \begin{bmatrix} \bar{\mathbf{S}}_{II}^L & \bar{\mathbf{S}}_{IO}^L \\ (\bar{\mathbf{S}}_{IO}^L)^T & \bar{\mathbf{S}}_{OO}^L \end{bmatrix}, \quad (102)$$

$$\bar{\alpha}^L = [\bar{\alpha}_i^L] = \begin{bmatrix} \bar{\alpha}_I^L \\ \bar{\alpha}_O^L \end{bmatrix}, \quad (103)$$

where

$$\bar{\mathbf{S}}_{II}^L = \left[\sum_{n=1}^N \frac{t_k}{t_L} (\bar{\mathbf{S}}_{II}^k)^{-1} \right]^{-1}, \quad (104)$$

$$\bar{\mathbf{S}}_{IO}^L = \bar{\mathbf{S}}_{II}^L \left[\sum_{n=1}^N \frac{t_k}{t_L} (\bar{\mathbf{S}}_{II}^k)^{-1} \bar{\mathbf{S}}_{IO}^k \right], \quad (105)$$

$$\bar{\mathbf{S}}_{\text{OO}}^L = (\bar{\mathbf{S}}_{\text{IO}}^L)^T (\bar{\mathbf{S}}_{\text{II}}^L)^{-1} \bar{\mathbf{S}}_{\text{IO}}^L + \sum_{n=1}^N \frac{t_k}{t_L} [\bar{\mathbf{S}}_{\text{OO}}^k - (\bar{\mathbf{S}}_{\text{IO}}^k)^T (\bar{\mathbf{S}}_{\text{II}}^k)^{-1} \bar{\mathbf{S}}_{\text{IO}}^k], \quad (106)$$

$$\bar{\boldsymbol{\alpha}}_i^L = \bar{\mathbf{S}}_{\text{II}}^L \left[\sum_{n=1}^N \frac{t_k}{t_L} (\bar{\mathbf{S}}_{\text{II}}^k)^{-1} \bar{\boldsymbol{\alpha}}_i^k \right], \quad (107)$$

$$\bar{\boldsymbol{\alpha}}_0^L = (\bar{\mathbf{S}}_{\text{IO}}^L)^T (\bar{\mathbf{S}}_{\text{II}}^L)^{-1} \bar{\boldsymbol{\alpha}}_i^L + \sum_{n=1}^N \frac{t_k}{t_L} [\bar{\boldsymbol{\alpha}}_0^k - (\bar{\mathbf{S}}_{\text{IO}}^k)^T (\bar{\mathbf{S}}_{\text{II}}^k)^{-1} \bar{\boldsymbol{\alpha}}_i^k], \quad (108)$$

where the 6×6 effective compliance matrices $\bar{\mathbf{S}}^k$ and $\bar{\mathbf{S}}^L$ are divided into 3×3 submatrices $\bar{\mathbf{S}}_m^k$ and $\bar{\mathbf{S}}_m^L$ ($m = \text{II}, \text{IO}, \text{OO}$), as indicated in Eqs. (96) and (102). Superscript L denotes the laminate components, and t_L is laminate thickness. From the effective compliance $\bar{\mathbf{S}}^L = [\bar{S}_{ij}^L]$ in Eq. (102) and the effective thermal expansion coefficient $\bar{\boldsymbol{\alpha}}^L = [\bar{\alpha}_i^L]$ in Eq. (103) of laminate with ply cracks, the effective thermo-elastic constants of the damaged laminate can be calculated as

$$E_X^L = \frac{1}{\bar{S}_{11}^L}, \quad E_Y^L = \frac{1}{\bar{S}_{22}^L}, \quad E_Z^L = \frac{1}{\bar{S}_{44}^L}, \quad (109)$$

$$\nu_{XY}^L = -\frac{\bar{S}_{12}^L}{\bar{S}_{11}^L}, \quad \nu_{XZ}^L = -\frac{\bar{S}_{14}^L}{\bar{S}_{11}^L}, \quad \nu_{YZ}^L = -\frac{\bar{S}_{24}^L}{\bar{S}_{22}^L}, \quad (110)$$

$$G_{XY}^L = \frac{1}{\bar{S}_{33}^L}, \quad G_{XZ}^L = \frac{1}{\bar{S}_{55}^L}, \quad G_{YZ}^L = \frac{1}{\bar{S}_{66}^L}, \quad (111)$$

$$\alpha_X^L = \bar{\alpha}_1^L, \quad \alpha_Y^L = \bar{\alpha}_2^L, \quad \alpha_Z^L = \bar{\alpha}_4^L, \quad (112)$$

$$\alpha_{XY}^L = \bar{\alpha}_3^L, \quad \alpha_{XZ}^L = \bar{\alpha}_5^L, \quad \alpha_{YZ}^L = \bar{\alpha}_6^L. \quad (113)$$

Using Eqs. (109)–(113), changes in the thermo-elastic properties of the laminate due to change in ply crack density are obtained analytically by determining the thermo-elastic properties of a ply and the laminated constitution, with no fitting parameter. The proposed model for predicting the thermo-elastic properties of the laminate is an analytical model of ply cracking in general composite laminates and exhibits favorable compatibility with laminate theory because it handles only damaged plies. The present model is not limited to symmetric laminates, including free surface; it formulates damage parameters ω and ξ analytically and therefore incurs little computational cost.

2.4. Steady-state cracking analysis

This subsection considers the energy-based model for steady-state ply cracking. Steady-state cracking is the fracture mode that a ply crack will propagate over the full-width of the specimen under constant thermomechanical loading. It is also assumed that a new ply crack propagates between two pre-existing cracks only in the k -th ply under constant applied laminate tensile stress, as indicated in Fig. 6, when the ply cracks are equally spaced. Ply crack density is defined as $\rho = 1/(2l)$.

With these assumptions, the energy release rate Γ^k associated with ply cracking in a k -th ply under constant applied laminate tensile stress $\bar{\boldsymbol{\sigma}}^L$ is

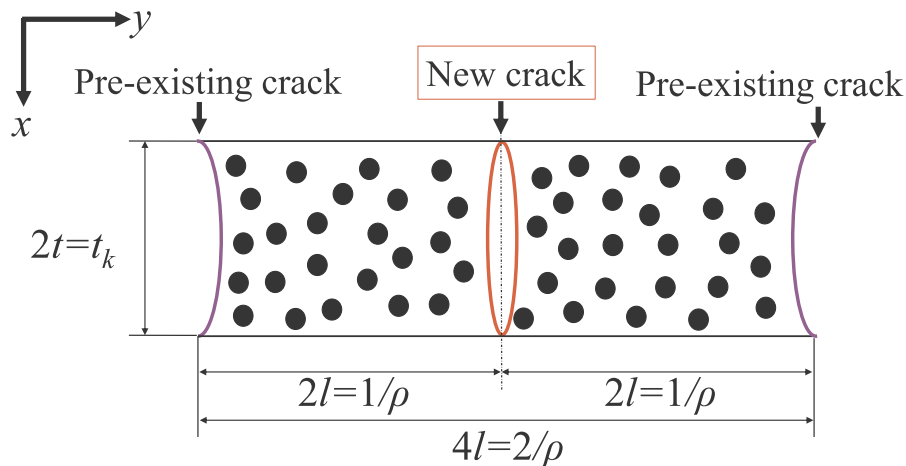


Fig. 6. Formation of a new crack between two pre-existing cracks in the k -th ply.

$$\Gamma^k(\rho) = -\frac{U^k(\rho/2) - 2U^k(\rho)}{t_k}, \quad (114)$$

where $U^k(\rho)$ is strain energy in a laminate with length $2l$ and laminate thickness t_L . The strain energy $U^k(\rho)$ is given by

$$U^k(\rho) = \frac{t_L}{2\rho} (\bar{\sigma}^L - \bar{\sigma}^{\text{th}})^T \bar{S}^L (\bar{\sigma}^L - \bar{\sigma}^{\text{th}}), \quad (115)$$

where $\bar{\sigma}^{\text{th}}$ is the laminate stress to cancel out the thermal residual stress of the k -th ply. When the thermomechanical loading $\bar{\sigma}^L$ of the laminate is equal to the stress $\bar{\sigma}^{\text{th}}$, all stress components of k -th ply are zero. The stress $\bar{\sigma}^{\text{th}}$ can be written as $\bar{\sigma}^{\text{th}} = [(\bar{\sigma}_1^{\text{th}})^T \ (\bar{\sigma}_0^{\text{th}})^T]^T$. Under this loading condition, $\bar{\sigma}_1^{\text{th}}$ and $\bar{\sigma}_0^{\text{th}}$ are calculated using the first row of Eqs. (C.1) and (C.2) and Eq. (C.3).

$$\bar{\sigma}_1^{\text{th}} = (\bar{S}_{11}^L)^{-1} (\bar{S}_{11}^k \bar{\sigma}_1^k + (\bar{S}_{10}^k - \bar{S}_{10}^L) \bar{\sigma}_0^{\text{th}} - (\bar{\alpha}_1^L - \bar{\alpha}_1^k) \Delta T), \quad (116)$$

$$\bar{\sigma}_0^{\text{th}} = \bar{\sigma}_0^k. \quad (117)$$

Substituting $\bar{\sigma}_1^k = \bar{\sigma}_0^k = 0$ into Eqs. (116) and (117), the stress $\bar{\sigma}^{\text{th}}$ is formulated as

$$\bar{\sigma}^{\text{th}} = \begin{bmatrix} \bar{\sigma}_1^{\text{th}} \\ \bar{\sigma}_0^{\text{th}} \end{bmatrix} = \begin{bmatrix} -(\bar{S}_{11}^L)^{-1} (\bar{\alpha}_1^L - \bar{\alpha}_1^k) \Delta T \\ 0 \end{bmatrix}. \quad (118)$$

The energy release rate Γ^k can be calculated substituting Eqs. (115) and (118) into Eq. (114). In this study, the uniaxial monotonic tensile stress $\sigma^{L,\text{app}}$ of the laminate is considered as

$$\bar{\sigma}^L = [\sigma^{L,\text{app}} \ 0 \ 0 \ 0 \ 0 \ 0]^T \quad (119)$$

Cracking analysis of the energy-based model for initiation of steady-state ply cracking in laminate is conducted as follows. It is assumed that ply cracks form in just one ply. Using Eq. (114), the energy release rate Γ^k of each ply is calculated as a function of ply crack density ρ at applied average laminate stress $\sigma^{L,\text{app}}$. The critical ply crack density ρ_k^c and the critical applied laminate stress $\sigma_c^{L,k}$ when the maximum value of the energy release rate $\max_{\rho}(\Gamma^k)$ associated with ply cracking in a k -th ply is equal to the critical energy release rate Γ^c are calculated. The ply having minimum cracking laminate stress $\min_k(\sigma_c^{L,k})$ is determined as steady-state cracking stress.

3. Results and discussion

The damage parameter ω has upper limit because the effective stiffness C in Eq. (4) is formulated by assuming small damage. Small damage refers to the condition in which the damage parameter ω is very small (i.e., $\omega^2 \ll 1$). It also means relatively low crack density because the damage parameter ω is a monotone increasing function of crack density. First, the upper limit of ω was investigated in the case of various CFRP and GFRP plies. Then, the proposed model was validated by calculating the effective thermoelastic properties and steady-state cracking stress in comparison with experiment and finite-element analysis (FEA) results in previous works on GFRP and CFRP laminates. The material properties of GFRP and CFRP unidirectional plies are listed in Table 1.

3.1. Maximum values of damage parameter and ply crack density

This subsection describes the upper limits of damage parameter ω and ply crack density. The effective stiffness C is valid while the approximate expression of shear stiffness reduction D_s in Eq. (81) is equal to that calculated using Eqs. (57) and (80). These upper limits can be obtained by comparing shear stiffness reduction D_s - damage parameter ω curve calculated using Eqs. (57) and (80) with that estimated using Eq. (81) for low damage conditions. Fig. 7 plots shear stiffness reduction D_s as a function of damage parameter ω for CFRP unidirectional ply listed in Table 1 calculated using Eqs. (57) and (80) or Eq. (81).

In the range of small ω , shear stiffness reduction D_s estimated using Eq. (81) is in good agreement with that calculated using Eqs. (57) and (80). A similar trend was observed for GFRP unidirectional plies. We determine that the damage parameter ω when the relative error of stiffness reduction D_s estimated using Eq. (81) to that calculated using Eqs. (57) and (80) is equal to 10 % is the upper limit of damage parameter ω . The upper limit of the damage parameter is converted into the maximum value of normalized crack

Table 1
Material properties of GFRP and CFRP unidirectional plies.

Type	E_1^0 (GPa)	E_2^0 (GPa)	ν_{12}^0	ν_{23}^0	G_{12}^0 (GPa)	G_{23}^0 (GPa)	α_1^0 (/°C)	α_2^0 (/°C)	Ply thickness (mm)
GFRP-1 [19]	41.7	13	0.3	0.42	3.4	4.58	6.72	29.3	0.203
							$\times 10^{-6}$	$\times 10^{-6}$	
GFRP-2 [24]	46	13	0.3	0.42	5	4.6	-	-	0.5
GFRP-3 [7]	44.7	12.7	0.297	0.3	5.8	4.885	-	-	0.125
CFRP [19]	142	9.85	0.3	0.46	4.48	3.37	-	-	0.127

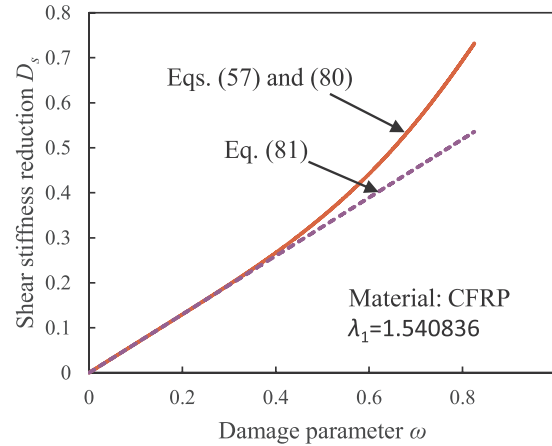


Fig. 7. Shear stiffness reduction D_s as a function of damage parameter ω for CFRP ply.

density, which is the product of crack density and ply thickness using Eq. (57). The maximum values of damage parameter ω_{\max} and normalized crack density $\rho_{N\max}$ for CFRP and GFRP plies in Table 1 are listed in Table 2.

The maximum value of damage parameter ω is approximately 0.57. For laminates that are used to calculate stiffness reduction, maximum crack densities ρ_{\max} ($\rho_{N\max}$ divided by ply thickness) are listed in Table 3.

The stiffness reduction of laminates with ply cracking was investigated in the range of maximum ply crack density ρ_{\max} listed in Table 3.

3.2. Cross-ply laminate

This subsection discusses the elastic modulus and the crack opening displacement of a cross-ply laminate with damage due to ply cracks or surface cracks in the 90° plies. Here $[90/0]_s$ GFRP laminate with surface cracks in the 90° plies was considered, and the material properties of GFRP-1 listed in Table 1 were used. Fig. 8(a) and (b) compare the results for the Young's modulus and Poisson's ratio of the laminate as a function of ply crack density as determined with the present model and previously published FEA results [19].

The results of the present model agree well with the FEA results. The normalized elastic moduli as a function of ply crack density of $[0/90]_s$ and $[0_2/90_2]_s$ CFRP laminates with ply cracks in the 90° plies are plotted in Figs. 9 and 10.

The experiment results [25] are also presented in Figs. 9 and 10. Here, E_X^{L0} is the elastic modulus in the X-direction of the undamaged laminate. The results obtained from the present model are in good agreement with the experiment results. Fig. 11 illustrates the normalized Young's modulus and normalized Poisson's ratio as a function of the ply crack density of $[0/90_8/0_{1/2}]_s$ GFRP laminate with ply cracks in the 90° plies as calculated by the present model, using the material properties of GFRP-3 listed in Table 1.

Here, ν_{XY}^{L0} is Poisson's ratio in the X – Y plane of the undamaged laminate. The experiment results [7] are also presented in Fig. 11. The results predicted by the present model were in good agreement with the experiment results. For cross-ply laminate, our model does not have an advantage over the simplistic shear-lag model. However, damage parameters derived in this paper are theoretical solutions under the assumption that the ply next to the cracked ply is rigid, and therefore the present model exhibits favorable compatibility with laminate theory that can be used to calculate the effective thermo-elastic constants of laminates with arbitrary lay-ups. Regarding this point, our model is superior to the shear-lag model that has difficulty solving the effective stiffness of damaged laminates for arbitrary lay-ups.

The crack opening displacement for $[0/90]_s$ CFRP laminate is compared with the semi-analytical results of the National Physical Laboratory (NPL) model calculated by McCartney et al. [26]. Using Eq. (47), the crack opening displacement v_{COD} can be calculated as

Table 2
Maximum value of damage parameter ω and normalized crack density $\rho_{N\max}$.

Material	ω_{\max}	$\rho_{N\max}$
CFRP	0.568	0.781
GFRP-1	0.569	0.788
GFRP-1 (surface crack)	0.569	0.394
GFRP-2	0.570	0.794
GFRP-3	0.577	0.832

Table 3
Maximum crack density of laminates used to calculate stiffness reduction.

Lay-up	Material	ρ_{\max} (/mm)
[90/0] _s	GFRP-1 (surface crack)	1.94
[0/90] _s	CFRP	3.07
[0 ₂ /90 ₂] _s	CFRP	1.54
[55/-55] _N	GFRP-1	3.88
[67.5/-67.5] _N	GFRP-1	3.88
[0/90/-45/+45] _s	GFRP-2	0.794
[0/90 ₈ /0 _{1/2}] _s	GFRP-3	0.832
[0/±70 ₄ /0 _{1/2}] _s	GFRP-3	1.66

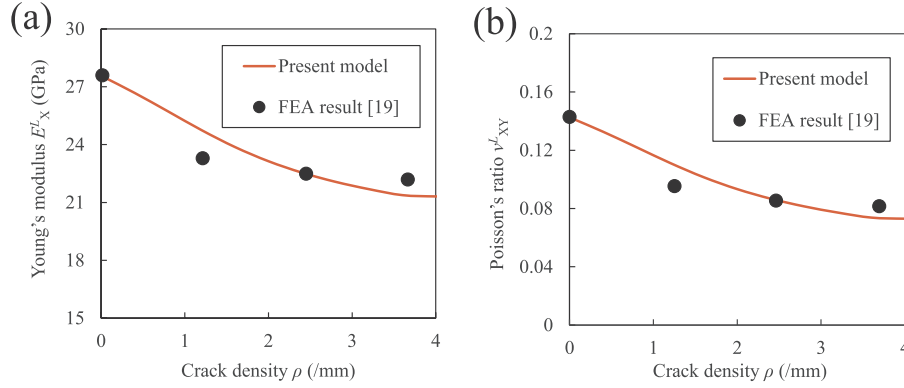


Fig. 8. (a) Young's modulus and (b) Poisson's ratio as a function of ply crack density for [90/0]_s GFRP laminate with surface cracks.

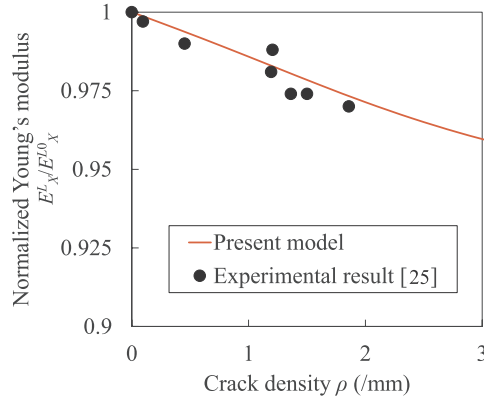


Fig. 9. Normalized Young's modulus as a function of ply crack density for [0/90]_s CFRP laminate with ply cracks.

$$\begin{aligned}
 v_{\text{COD}} &= 2[l\varepsilon_2^{\text{app}} - v(x, l, z)] \\
 &= 2 \left[1 - \frac{8l}{\pi^2} \sum_{n=1}^{\infty} \frac{1}{(2n-1)^2} \frac{\cosh[(2n-1)\pi\lambda_1 x / (2l)]}{\cosh[(2n-1)\pi\lambda_1 l / (2l)]} \right] l\varepsilon_2^{\text{app}}.
 \end{aligned} \tag{120}$$

The following material properties are used in the calculation of the crack opening displacement: $E_1 = 144.78$ GPa, $E_2 = 9.58$ GPa, $G_{12} = 4.785$ GPa, $\nu_{12} = 0.31$, $\nu_{23} = 0.55$, and $2t = 0.25$ mm. Crack opening displacement in 90° ply for CFRP [0/90]_s laminate at crack spacing $2l = 4.0$ mm and applied laminate stress $\sigma^{L,\text{app}} = 0.2$ GPa is plotted in Fig. 12.

The crack opening displacement calculated by the present model is less than that computed by the NPL model because our local stress field models or damage parameters did not consider stress transfer at the interface. It is assumed that the plies adjacent to the cracked ply are deformed uniformly in our model. Based on this assumption, the crack opening displacement in our model is less than that in the NPL model, which considers stress transfer at the interface. Our model takes into account stress transfer by reconsidering the boundary conditions of Laplace equations for v and w in Eqs. (46) and (75). This improvement of our model is our main future work.

There are many stiffness reduction models for cross-ply laminates. Lee et al. [14] derived stiffness reductions in cross-ply

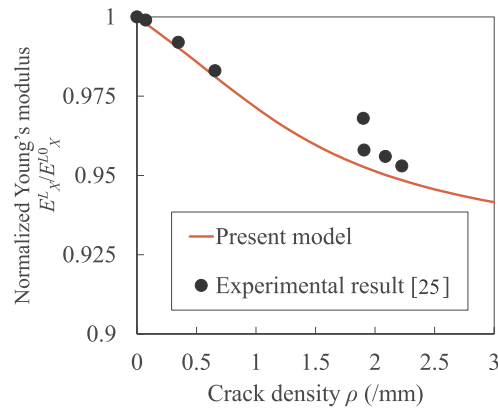


Fig. 10. Normalized Young's modulus as a function of ply crack density for $[0_2/90_2]_s$ CFRP laminate with ply cracks.

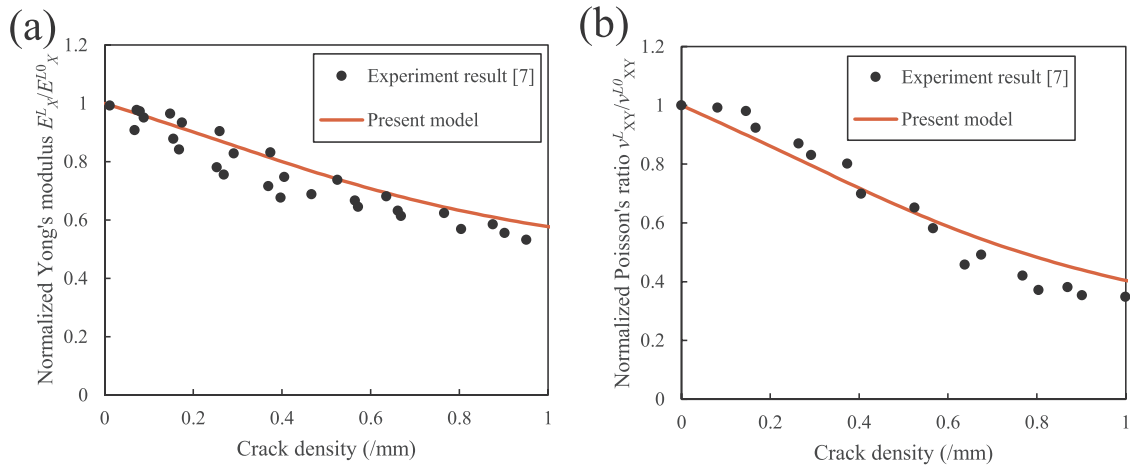


Fig. 11. (a) Normalized Young's modulus and (b) normalized Poisson's ratio as a function of ply crack density for $[0/90_8/0_{1/2}]_s$ GFRP laminate with ply cracks.

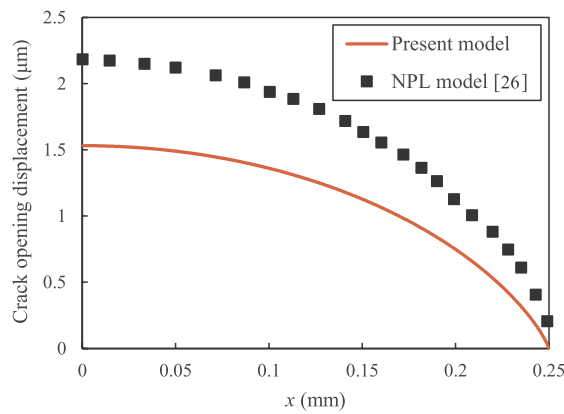


Fig. 12. Crack opening displacement in 90° ply for CFRP $[0/90]_s$ laminate at crack spacing $2l = 4.0$ mm and applied laminate stress $\sigma^{L,app} = 0.2$ GPa.

laminates with ply cracks using an internal state variable approach. They formulated an internal state variable that describes the damage state in composite materials using a stress field model of cross-ply laminates including ply cracks. However, this stress field model does not satisfy the stress-free condition at the crack plane. Therefore, their model overestimated the stiffness of laminates. In contrast, our local stress field models fulfilled the stress-free condition on the crack plane. One- or two-dimensional shear-lag analyses [27] have been very useful for approximating the stress transfer at the interface by shear stress. However, shear-lag models must be confined to symmetric laminates and symmetric damage, because they neglect the bending effect in their formulations. For example,

Nairn and Hu [28] formulated $[90_m/0_n]_s$ laminate including staggered ply cracks using variational mechanics analysis of the stresses. For $[90_m/0_n]_s$ laminates, these shear-lag analyses were inadequate because antisymmetric or staggered ply cracks were observed in experiments. Although other variational models [4,28–30] (e.g., the Nairn and Hu model) can treat laminates including staggered ply cracks, these models are limited to simplified laminate configurations. In contrast, our model can handle the staggered ply crack pattern and can consider laminates with any configuration. Gudmundson and Zang [19] derived a general three-dimensional laminate model with ply cracks based on crack opening displacements, and their model can predict the average stress in each ply. However, the local stress field in a ply is not included in their model, whereas our model can analytically predict the local stress field model in 90° plies, as indicated in Eqs. (47)–(52).

3.3. Angle-ply laminate

This subsection discusses all the effective thermoelastic properties of angle-ply GFRP laminates of $[\pm 55]_N$ and $[\pm 67.5]_N$ that include ply cracks in each ply. The material properties of GFRP-1 listed in Table 1 were used in the calculations, and Figs. 13 and 14 present the Young’s moduli, shear moduli, Poisson’s ratios, and thermal expansion coefficients for $[\pm 55]_N$ and $[\pm 67.5]_N$ laminates as functions of ply crack density estimated using the present model or FEA results [19].

For $[\pm 55]_N$ and $[\pm 67.5]_N$ laminates, the behavior predicted by the present model is approximately equal to that of the FEA results. Fig. 15 indicates the normalized Young’s modulus and normalized Poisson’s ratio as a function of crack density of $[0/\pm 70_4/0_{1/2}]_s$ GFRP laminate with ply cracking in $\pm 70^\circ$ plies as calculated by the present model, using the material properties of GFRP-3 listed in Table 1.

The experiment results by Varna et al. [7] are also presented in Fig. 15. Their experiment results are much smaller than the results of our model when crack density exceeds 0.2/mm. The stiffness of the experiment results declines drastically when crack density increases from 0.2/mm to 0.4/mm. The formation of local delamination is cited as a possible cause of the difference between the present model and the experiment results. Experiment observation [31] indicates that matrix crack-induced delamination or edge delamination occurs in the angle-ply laminates. Furthermore, as pointed out in [7,8], stiffness reduction for the $[0/\pm \theta_4/0_{1/2}]_s$ GFRP angle-ply laminate is due to ply cracking as well as shear-induced damage depending on the angle θ .

For angle-ply laminates, Vinogradov and Hashin [6] modeled $[\theta_m^{(1)}/\theta_n^{(2)}]$ laminates containing ply cracks in the middle ply using the

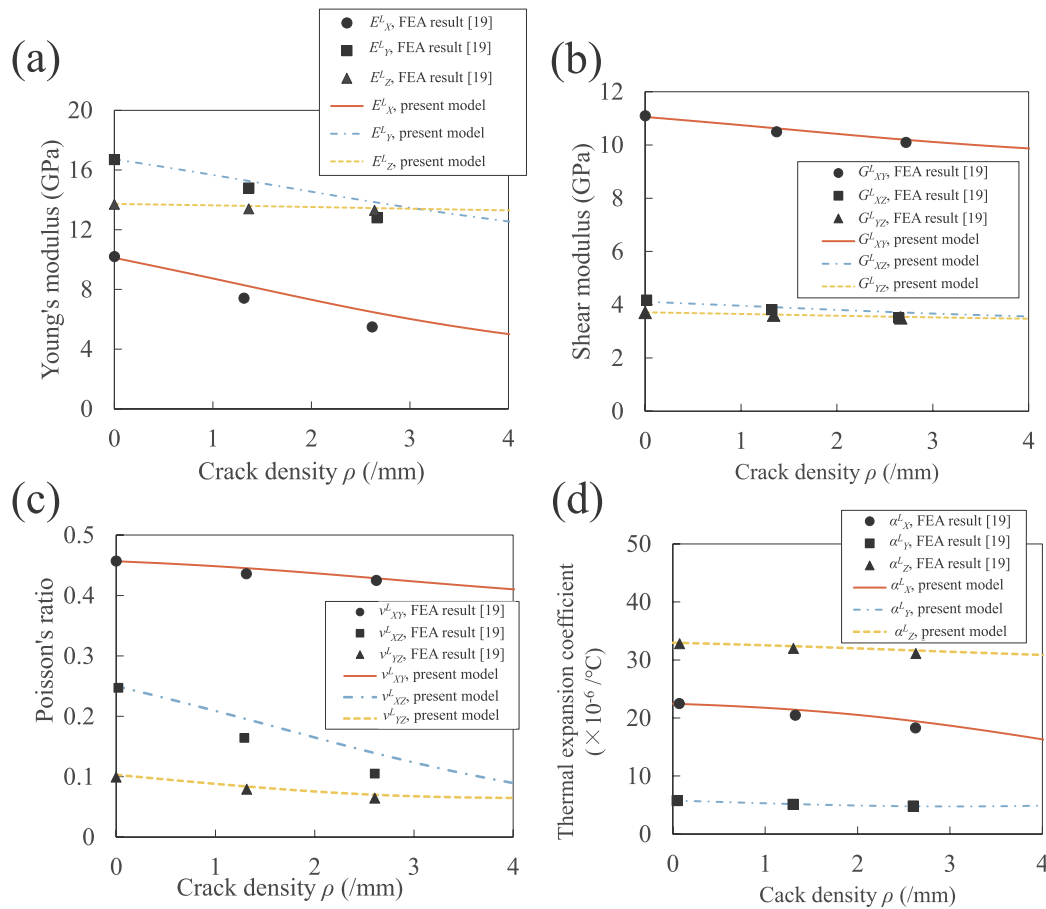


Fig. 13. (a) Young’s modulus, (b) shear modulus, (c) Poisson’s ratio, and (d) thermal expansion coefficient as a function of ply crack density for $[55/-55]_N$ GFRP laminate with ply cracks.

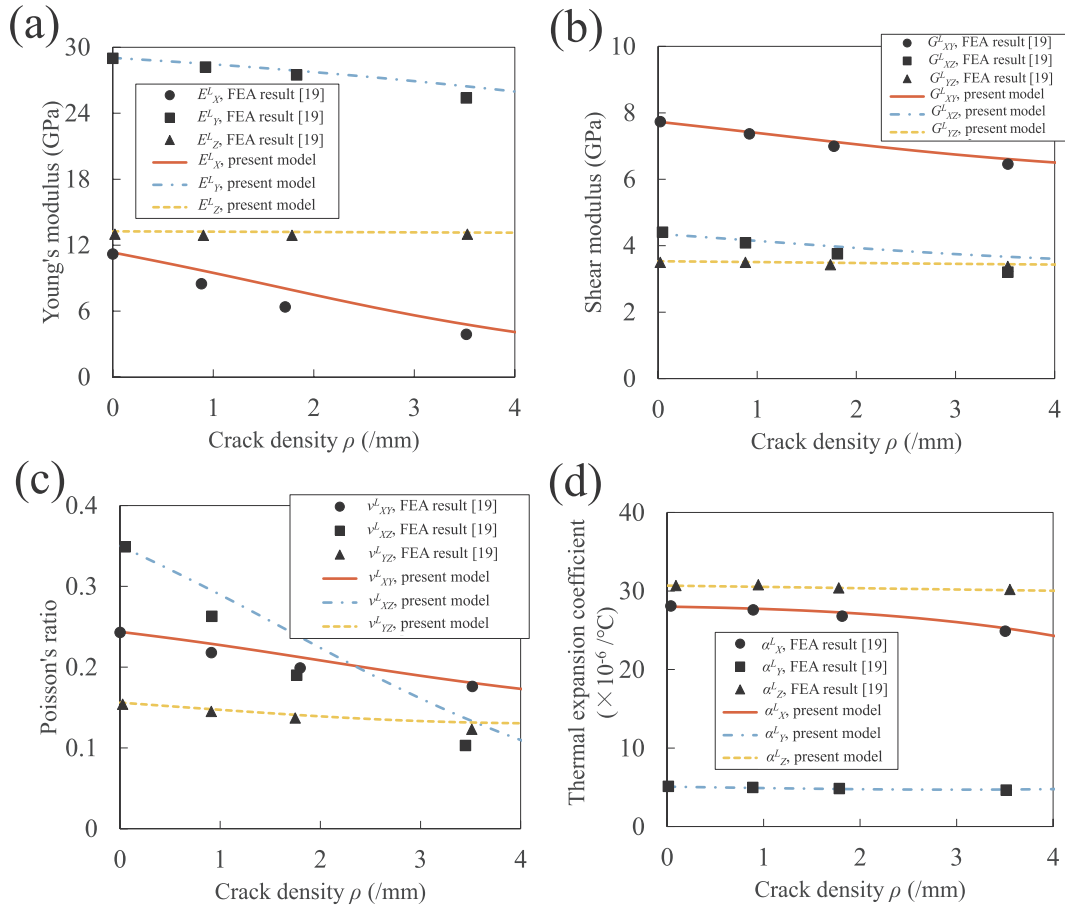


Fig. 14. (a) Young's modulus, (b) shear modulus, (c) Poisson's ratio, and (d) thermal expansion coefficient as a function of ply crack density for $[67.5/-67.5]_N$ GFRP laminate with ply cracks.

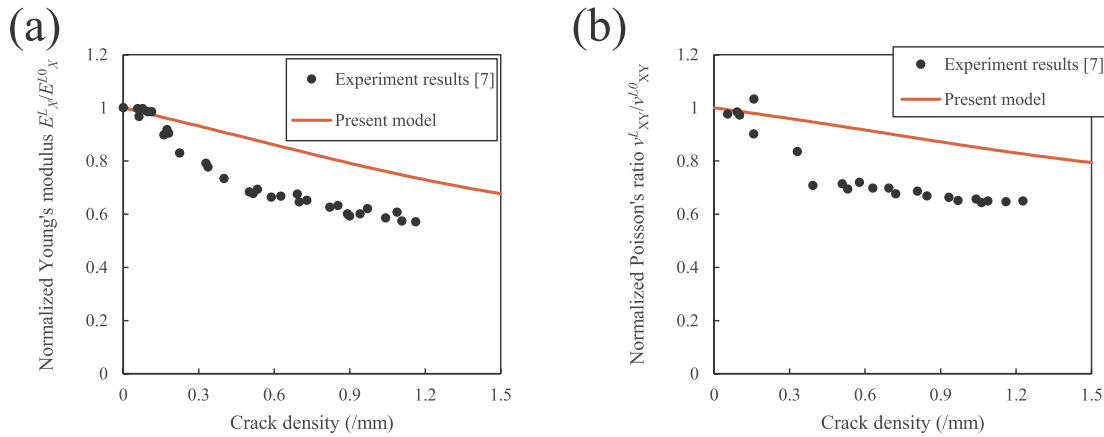


Fig. 15. (a) Normalized Young's modulus and (b) Normalized Poisson's ratio as a function of ply crack density for $[0/\pm 70_4/0_{1/2}]_S$ GFRP laminate.

principle of minimum complementary energy. Their model underestimated the stiffness of $[0_m/\theta_n]_s$ angle-ply laminates in comparison with experiment results [32], because the principle of minimum complementary energy provided a lower bound for the stiffness of a cracked angle-ply. Gudmundson and Zang [19] and Lundmark and Varna [33–35] formulated the effective properties of laminates with ply cracks using crack opening displacement-based methods, which describe the elastic response changes caused by ply cracks in a medium by considering the crack opening displacements of individual cracks. In Gudmundson and Zang's model, crack opening displacement was calculated by fitting the homogeneous isotropic medium with cracks under the action of uniform tractions on crack

surfaces given by Benthem and Koiter [36] and Tada et al. [37]. In the model formulated by Lundmark and Varna, crack opening displacement was computed by fitting empirical results with finite-element calculations. In contrast, our stress field model analytically derived the crack opening displacement in the transversely isotropic elastic body from the displacement.

3.4. Quasi-isotropic laminate

The quasi-isotropic $[0/90/-45/+45]_s$ GFRP laminate was analyzed to compare the results of our model with the experiment results obtained by Tong et al. [38], using the material properties of GFRP-2 listed in Table 1. We assume that all plies except 0° plies have the same damage, because the crack density in $\pm 45^\circ$ plies is not available from the experiment of Tong et al. With this assumption, the effective stiffness calculated by the present model is the lower bound because cracks in $\pm 45^\circ$ plies do not propagate perfectly through the laminate width, and cracks in $\pm 45^\circ$ initiate later than in 90° and contribute little to total stiffness reduction. Fig. 16 plots the normalized Young's modulus and normalized Poisson's ratio for the laminate obtained from the proposed model in comparison with the experiment results.

Although the contribution of $\pm 45^\circ$ cracks to laminate stiffness reduction is small, the effective Young's modulus of laminate obtained by our model is in good agreement with those of the experimental results. Fig. 16 is also plotted the result of present model without $\pm 45^\circ$ cracks. The present model without $\pm 45^\circ$ cracks is slightly higher than the experimental results at the range of crack density from 0/mm to 0.7/mm although the $\pm 45^\circ$ cracks did not cause at this range [38]. This reason is possibly due to local delamination at the crack tips.

A stiffness reduction model of quasi-isotropic laminates must be formulated, because most laminates used in real structures are quasi-isotropic. However, few analytical models enable such predictions [10,11,17]. Tay and Lim [17] suggested a stiffness reduction model of general laminates including ply cracks, using internal state variables that were fitted by finite-element calculation. McCartney [11] derived the stiffness reduction and progressive ply crack formation of general symmetric laminates with ply cracks using a generalized plane strain analysis and the homogenization technique, and considering the stress transfer at the interfaces of neighboring plies. However, this model could not be applied to asymmetric laminates, whereas the proposed model can predict the stiffness reduction of laminates with arbitrary configurations.

3.5. Steady-state cracking stress of cross-ply laminates

Steady-state cracking stress of cross-ply laminate estimated by the energy-based model described in Section 2.4 is compared with analytical results in previous studies. Here, $[0/90_m/0]$ ($m = 1, 2, 3, 4$) cross-ply laminate of IM7/5250 is analyzed; properties of the ply are listed in Table 4.

Fig. 17 plots steady-state cracking stress assuming steady-state cracking as a function of thickness of 90° plies per thickness of 0° plies.

For comparison, the analytical results using Gudmundson and Zang's [19] model's effective compliance matrix and the energy-based model (Eq. (114)) in this study are also plotted in Fig. 17. Furthermore, Fig. 17 includes the semi-analytical results of the NPL model [39] and the Large Radius Axisymmetric Damage Model (LRAM) [39], as well as the analytical results of Dvorak and Laws [40]. The present model is in quantitatively good agreement with the analytical results of the LRAM and NPL models [26,41]. Both semi-analytical models consider the stress transfer of neighboring ply caused by ply cracking. The LRAM model was developed by Schoeppner and Pagano [42] to approximate the thermoelastic stress field and energy release rate in flat laminates with ply cracks and delaminations. When the radius-to-laminate thickness ratio is equal to 100,000, the large radius axisymmetric damage model is reasonably similar to the stress fields and stiffness reduction of flat laminates estimated by the NPL model, which is considered to be the most accurate generalized plane strain model. Our damage mechanics model is formulated explicitly and is highly simplified,

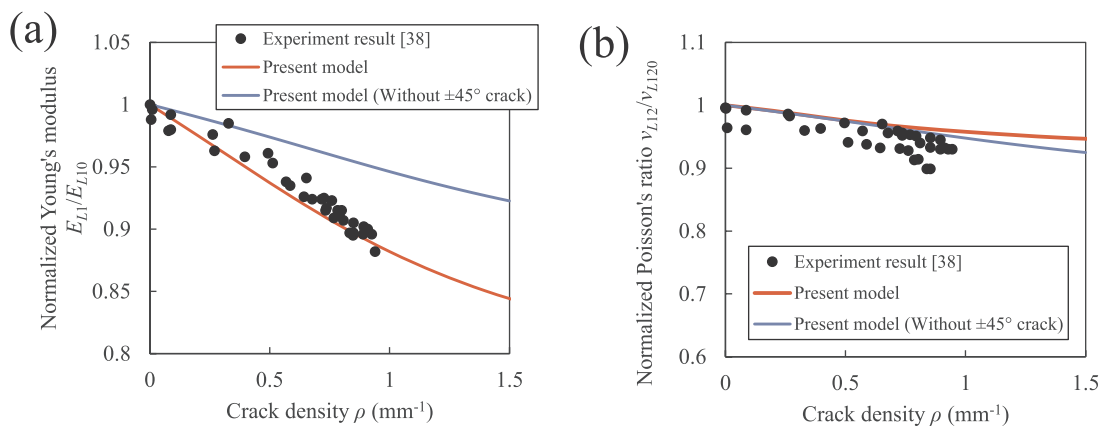


Fig. 16. (a) Normalized Young's modulus and (b) normalized Poisson's ratio as a function of ply crack density for $[0/90/-45/+45]_s$ GFRP laminate with ply cracks in 90° and $+45^\circ$ plies.

Table 4
Material properties of IM7/5250-4 [39].

Longitudinal Young's modulus E_1^0	165.475 GPa
Transverse Young's modulus E_2^0	10.342 GPa
In-plane Poisson's ratio ν_{12}^0	0.31
Out-of-plane Poisson's ratio ν_{23}^0	0.56
In-plane shear modulus G_{12}^0	5.7922 GPa
Out-of-plane shear modulus G_{23}^0	3.3147 GPa
Longitudinal thermal expansion coefficient α_1^0	$0.45 \times 10^{-6} / ^\circ\text{C}$
Transverse thermal expansion coefficient α_2^0	$24.66 \times 10^{-6} / ^\circ\text{C}$
Stress-free temperature T_{sf}	180 °C
Ambient testing temperature T	24 °C
Ply thickness	0.127 mm
Critical energy release Rate Γ_c	225 J/m ²

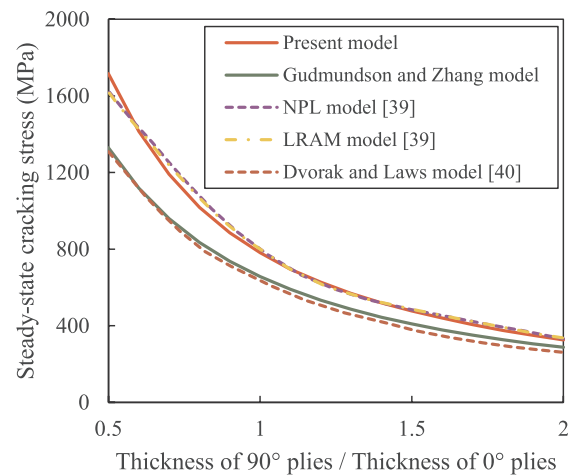


Fig. 17. Laminate crack initiation stress assuming steady-state cracking as a function of thickness of 90° plies per thickness of 0° plies.

whereas the LRAM and NPL models should solve the simultaneous differential equation numerically. The steady-state analytical results of Gudmundson and Zang's model and those of Dvorak and Laws's model are lower than the results of the present model, the LRAM, and the NPL model. Gudmundson and Zang's model and Dvorak and Laws's model assume that a cracked ply is identical to the infinite cracked medium. This assumption does not work well, because cracked ply in laminate is significantly constrained by adjacent plies. Therefore, the crack opening displacements of those models are higher than those of the other three models described here. In this study, we validated the present steady-state cracking analysis model by comparing it to semi-analytical and analytical results for cross-ply laminates, because there is an abundance of models for cross-ply laminate. The present model can be used to calculate crack density evolution for laminates with any lay-up. This is our future work, and we plan to publish the cracking analysis of laminate with any lay-up in our next paper.

4. Conclusions

In this study, the effective compliance and elastic constants of laminates were formulated based on a CDM approach and laminate theory, in an effort to predict the thermoelastic properties of laminates of arbitrary configurations as a function of ply crack density. The damage parameters ω and ξ were expressed as functions of ply crack density based on analytically formulated local stress field models subjected to tensile loading and shear loading. The model proposed in this study considers the effect of damage due to ply cracks (or surface cracks) based on only the thermomechanical properties of the ply and the laminate constitution. This model quantitatively reproduced FEA and experiment results for the thermomechanical properties of cross-ply, angle-ply, and quasi-isotropic laminates including ply cracks. Following the approach of energy-based steady-state cracking analysis, the laminate crack initiation stress for cross-ply is calculated and compared with analytical results in previous studies. Our model is quantitatively in good agreement with the semi-analytical results of the large radius axisymmetric damage model by Pagano and the NPL model by McCartney.

follows:

$$P_{kl} = \begin{cases} 1 & (k = l, k \neq i, k \neq j) \\ 1 & (k = i, l = j) \\ 1 & (k = j, l = i) \\ 0 & (\text{other}) \end{cases}. \quad (\text{B.4})$$

The nature of elementary matrix $P(i, j)$ is

$$P^{-1}(i, j) = P(i, j), \quad (\text{B.5})$$

$$P^T(i, j) = P(i, j). \quad (\text{B.6})$$

Using Eqs. (B.5) and (B.6), the inverse matrix of A can be calculated as

$$A^{-1} = A^T. \quad (\text{B.7})$$

Substituting Eqs. (B.1), (B.2), and (B.7) into Eq. (A.8), the constitutive law between the stress and strain in Eq. (91) is expressed as

$$\bar{\epsilon}^k = \bar{S}^k \bar{\sigma}^k + \bar{\alpha}^k \Delta T, \quad (\text{B.8})$$

where the effective compliance matrix \bar{S}^k and the thermal expansion coefficient $\bar{\alpha}^k$ of the k -th ply for $\bar{\sigma}^k$ and $\bar{\epsilon}^k$ are indicated in Eqs. (96) and (97). The compliance matrix S^k of the orthotropic plate is described as

$$S^k = \begin{bmatrix} S_{11}^k & S_{12}^k & S_{13}^k & 0 & 0 & S_{16}^k \\ S_{12}^k & S_{22}^k & S_{23}^k & 0 & 0 & S_{26}^k \\ S_{13}^k & S_{23}^k & S_{33}^k & 0 & 0 & S_{36}^k \\ 0 & 0 & 0 & S_{44}^k & S_{45}^k & 0 \\ 0 & 0 & 0 & S_{45}^k & S_{55}^k & 0 \\ S_{16}^k & S_{26}^k & S_{36}^k & 0 & 0 & S_{66}^k \end{bmatrix}. \quad (\text{B.9})$$

Substituting Eq. (B.9) into Eq. (96), the compliance matrix \bar{S}^k can be expressed as

$$\bar{S}^k = \begin{bmatrix} S_{11}^k & S_{12}^k & S_{16}^k & S_{13}^k & 0 & 0 \\ S_{12}^k & S_{22}^k & S_{26}^k & S_{23}^k & 0 & 0 \\ S_{16}^k & S_{26}^k & S_{66}^k & S_{36}^k & 0 & 0 \\ S_{13}^k & S_{23}^k & S_{36}^k & S_{33}^k & 0 & 0 \\ 0 & 0 & 0 & 0 & S_{55}^k & S_{45}^k \\ 0 & 0 & 0 & 0 & S_{45}^k & S_{44}^k \end{bmatrix}. \quad (\text{B.10})$$

Appendix C. Formulation of the three-dimensional laminate theory

The three-dimensional laminate theory is utilized to formulate the thermoelastic properties of the composite laminate. The constitutive law of the laminate for average stress and strain in Eq. (99) is expressed as

$$\bar{\epsilon}^L = \begin{bmatrix} \bar{\epsilon}_I^L \\ \bar{\epsilon}_O^L \end{bmatrix} = \bar{S}^L \bar{\sigma}^L + \bar{\alpha}^L \Delta T = \begin{bmatrix} \bar{S}_{II}^L & \bar{S}_{IO}^L \\ (\bar{S}_{IO}^L)^T & \bar{S}_{OO}^L \end{bmatrix} \begin{bmatrix} \bar{\sigma}_I^L \\ \bar{\sigma}_O^L \end{bmatrix} + \begin{bmatrix} \bar{\alpha}_I^L \\ \bar{\alpha}_O^L \end{bmatrix} \Delta T, \quad (\text{C.1})$$

and the constitutive law of the k -th ply for average stress and strain in Eq. (91) is given by

$$\bar{\epsilon}^k = \begin{bmatrix} \bar{\epsilon}_I^k \\ \bar{\epsilon}_O^k \end{bmatrix} = \bar{S}^k \bar{\sigma}^k + \bar{\alpha}^k \Delta T = \begin{bmatrix} \bar{S}_{II}^k & \bar{S}_{IO}^k \\ (\bar{S}_{IO}^k)^T & \bar{S}_{OO}^k \end{bmatrix} \begin{bmatrix} \bar{\sigma}_I^k \\ \bar{\sigma}_O^k \end{bmatrix} + \begin{bmatrix} \bar{\alpha}_I^k \\ \bar{\alpha}_O^k \end{bmatrix} \Delta T, \quad (\text{C.2})$$

where superscript L denotes the laminate component and k denotes the k -th ply component. From the compatibility and equilibrium conditions in the laminate, the following relationships must be satisfied.

$$\bar{\epsilon}_I^k = \bar{\epsilon}_I^L, \quad \bar{\sigma}_O^k = \bar{\sigma}_O^L \quad (\text{C.3})$$

The laminate average stresses and strains are defined as

$$\bar{\sigma}^L = \begin{bmatrix} \bar{\sigma}_I^L \\ \bar{\sigma}_O^L \end{bmatrix} = \sum_{k=1}^N \frac{t_k}{t_L} \bar{\sigma}^k = \sum_{k=1}^N \frac{t_k}{t_L} \begin{bmatrix} \bar{\sigma}_I^k \\ \bar{\sigma}_O^k \end{bmatrix}, \quad (\text{C.4})$$

$$\bar{\varepsilon}^L = \begin{bmatrix} \bar{\varepsilon}_1^L \\ \bar{\varepsilon}_0^L \end{bmatrix} = \sum_{k=1}^N \frac{t_k}{t_L} \bar{\varepsilon}^k = \sum_{k=1}^N \frac{t_k}{t_L} \begin{bmatrix} \bar{\varepsilon}_1^k \\ \bar{\varepsilon}_0^k \end{bmatrix}, \quad (\text{C.5})$$

where

$$t_L = \sum_{k=1}^N t_k. \quad (\text{C.6})$$

Here, t_L is laminate thickness, and t_k is k -th ply thickness. From the first row of Eqs. (C.2) and (C.3), in-plane average stress of k -th ply $\bar{\sigma}_1^k$ can be obtained as

$$\bar{\sigma}_1^k = (\bar{\mathcal{S}}_{11}^k)^{-1}(\bar{\varepsilon}_1^L - \bar{\mathcal{S}}_{10}^k \bar{\sigma}_0^L - \bar{\alpha}_1^k \Delta T). \quad (\text{C.7})$$

Substituting Eq. (C.7) into the first row of Eq. (C.4), the in-plane average laminate strain $\bar{\varepsilon}_1^L$ is expressed as

$$\begin{aligned} \bar{\varepsilon}_1^L = & \left[\sum_{k=1}^N \frac{t_k}{t_L} (\bar{\mathcal{S}}_{11}^k)^{-1} \right]^{-1} \bar{\sigma}_1^L + \left[\sum_{k=1}^N \frac{t_k}{t_L} (\bar{\mathcal{S}}_{11}^k)^{-1} \right]^{-1} \left[\sum_{k=1}^N \frac{t_k}{t_L} (\bar{\mathcal{S}}_{11}^k)^{-1} \bar{\mathcal{S}}_{10}^k \right] \bar{\sigma}_0^L \\ & + \left[\sum_{k=1}^N \frac{t_k}{t_L} (\bar{\mathcal{S}}_{11}^k)^{-1} \right]^{-1} \left[\sum_{k=1}^N \frac{t_k}{t_L} (\bar{\mathcal{S}}_{11}^k)^{-1} \bar{\alpha}_1^k \right] \Delta T. \end{aligned} \quad (\text{C.8})$$

By comparing Eq. (C.8) and the first row of Eq. (C.1), the compliance submatrices of the laminate $\bar{\mathcal{S}}_{11}^L$ and $\bar{\mathcal{S}}_{10}^L$ and in-plane thermal expansion coefficient of laminate $\bar{\alpha}_1^L$ are obtained as Eqs. (104), (105), and (107). In terms of the out-of-plane components, from the second row of Eqs. (C.2) and (C.3), the out-of-plane average strain of k -th ply $\bar{\varepsilon}_0^k$ is formulated as

$$\bar{\varepsilon}_0^k = (\bar{\mathcal{S}}_{10}^k)^T \bar{\sigma}_1^k + \bar{\mathcal{S}}_{00}^k \bar{\sigma}_0^L + \bar{\alpha}_0^k \Delta T. \quad (\text{C.9})$$

Inserting Eq. (C.9) into the second row of Eq. (C.5) and using Eq. (C.7) and the first row of Eq. (C.1), the out-of-plane average strain of laminate can be expressed as

$$\begin{aligned} \bar{\varepsilon}_0^L = & \sum_{k=1}^N \frac{t_k}{t_L} [(\bar{\mathcal{S}}_{10}^k)^T (\bar{\mathcal{S}}_{11}^k)^{-1} \bar{\mathcal{S}}_{11}^L \bar{\sigma}_1^L \\ & + \{(\bar{\mathcal{S}}_{10}^k)^T (\bar{\mathcal{S}}_{11}^k)^{-1} (\bar{\mathcal{S}}_{10}^L - \bar{\mathcal{S}}_{10}^k) + \bar{\mathcal{S}}_{00}^k\} \bar{\sigma}_0^L \\ & + \{(\bar{\mathcal{S}}_{10}^k)^T (\bar{\mathcal{S}}_{11}^k)^{-1} (\bar{\alpha}_1^L - \bar{\alpha}_1^k) + \bar{\alpha}_0^k\} \Delta T]. \end{aligned} \quad (\text{C.10})$$

The following relationship can be obtained using Eq. (105).

$$\sum_{k=1}^N \frac{t_k}{t_L} (\bar{\mathcal{S}}_{10}^k)^T (\bar{\mathcal{S}}_{11}^k)^{-1} = (\bar{\mathcal{S}}_{10}^L)^T (\bar{\mathcal{S}}_{11}^L)^{-1} \quad (\text{C.11})$$

Substituting Eq. (C.11) into Eq. (C.10), the out-of-plane average strain of laminate is rewritten as

$$\begin{aligned} \bar{\varepsilon}_0^L = & (\bar{\mathcal{S}}_{10}^L)^T \bar{\sigma}_1^L \\ & + \left[(\bar{\mathcal{S}}_{10}^L)^T (\bar{\mathcal{S}}_{11}^L)^{-1} \bar{\mathcal{S}}_{10}^L + \sum_{k=1}^N \frac{t_k}{t_L} (\bar{\mathcal{S}}_{00}^k - (\bar{\mathcal{S}}_{10}^k)^T (\bar{\mathcal{S}}_{11}^k)^{-1} \bar{\mathcal{S}}_{10}^k) \right] \bar{\sigma}_0^L \\ & + \left[(\bar{\mathcal{S}}_{10}^L)^T (\bar{\mathcal{S}}_{11}^L)^{-1} \bar{\alpha}_1^L + \sum_{k=1}^N \frac{t_k}{t_L} (\bar{\alpha}_0^k - (\bar{\mathcal{S}}_{10}^k)^T (\bar{\mathcal{S}}_{11}^k)^{-1} \bar{\alpha}_1^k) \right] \Delta T. \end{aligned} \quad (\text{C.12})$$

By comparing Eq. (C.12) and the second row of Eq. (C.1), the compliance submatrix of the laminate $\bar{\mathcal{S}}_{00}^L$ and out-of-plane thermal expansion coefficient of laminate $\bar{\alpha}_0^L$ are obtained as Eqs. (106) and (108).

References

- [1] Nairn J, Hu S. Micromechanics of damage: a case study of matrix microcracking. In: Talreja R, editor. *Damage mechanics of composite materials*. Amsterdam: Elsevier; 1994. p. 187–243.
- [2] Takeda N, Ogihara S. In situ observation and probabilistic prediction of microscopic failure processes in CFRP cross-ply laminates. *Compos Sci Technol* 1994;52:183–95. [https://doi.org/10.1016/0266-3538\(94\)90204-6](https://doi.org/10.1016/0266-3538(94)90204-6).
- [3] Talreja R, Singh C. *Damage and failure of composite materials*. New York: Cambridge University Press; 2012. <https://doi.org/10.1017/CBO9781139016063>.
- [4] Hashin Z. Analysis of cracked laminates: a variational approach. *Mech Mater* 1985;4:121–36. [https://doi.org/10.1016/0167-6636\(85\)90011-0](https://doi.org/10.1016/0167-6636(85)90011-0).
- [5] McCartney L. Theory of stress transfer in a 0°-90°-0° cross-ply laminate containing a parallel array of transverse cracks. *J Mech Phys Solids* 1992;40:27–68. [https://doi.org/10.1016/0022-5096\(92\)90226-R](https://doi.org/10.1016/0022-5096(92)90226-R).
- [6] Vinogradov V, Hashin Z. Variational analysis of cracked angle-ply laminates. *Compos Sci Technol* 2010;70:638–46. <https://doi.org/10.1016/j.compscitech.2009.12.018>.
- [7] Varna J, Joffe R, Akshantala N, Talreja R. Damage in composite laminates with off-axis plies. *Compos Sci Technol* 1999;59:2139–47. [https://doi.org/10.1016/S0266-3538\(99\)00070-6](https://doi.org/10.1016/S0266-3538(99)00070-6).

- [8] Singh CV, Talreja R. Analysis of multiple off-axis ply cracks in composite laminates. *Int J Solids Struct* 2008;45:4574–89. <https://doi.org/10.1016/j.ijsolstr.2008.04.004>.
- [9] Hajikazemi M, McCartney L, Van Paepegem W, Sadr M. Theory of variational stress transfer in general symmetric composite laminates containing non-uniformly spaced ply cracks. *Compos Part A: Appl Sci Manuf* 2018;107:374–86. <https://doi.org/10.1016/j.compositesa.2018.01.021>.
- [10] Hajikazemi M, McCartney L. Comparison of Variational and Generalized Plane Strain approaches for matrix cracking in general symmetric laminates. *Int J Damage Mech* 2018;27:507–40. <https://doi.org/10.1177/1056789516685381>.
- [11] McCartney L. Model to predict effects of triaxial loading on ply cracking in general symmetric laminates. *Compos Sci Technol* 2000;60:2255–79. [https://doi.org/10.1016/S0266-3538\(00\)00086-5](https://doi.org/10.1016/S0266-3538(00)00086-5).
- [12] Allen D, Harris C, Groves S. A thermomechanical constitutive theory for elastic composites with distributed damage-I. Theoretical development. *Int J Solids Struct* 1987;23:1301–18. [https://doi.org/10.1016/0020-7683\(87\)90107-7](https://doi.org/10.1016/0020-7683(87)90107-7).
- [13] Murakami S. *Continuum damage mechanics*. Dordrecht: Springer; 2012. <https://doi.org/10.1007/978-94-007-2666-6>.
- [14] Lee J-W, Allen D, Harris C. Internal state variable approach for predicting stiffness reductions in fibrous laminated composites with matrix cracks. *J Compos Mater* 1989;23:1273–91. <https://doi.org/10.1177/002199838902301205>.
- [15] Okabe T, Onodera S, Kumagai Y, Nagumo Y. Continuum damage mechanics modeling of composite laminates including transverse cracks. *Int J Damage Mech* 2018;27:877–95. <https://doi.org/10.1177/1056789517711238>.
- [16] Talreja R. A continuum mechanics characterization of damage in composite materials. *Proc Roy Soc Lond, Ser A: Math Phys Sci* 1985;399:195–216. <https://doi.org/10.1098/rspa.1985.0055>.
- [17] Tay T, Lim E. Analysis of composite laminates with transverse cracks. *Compos Struct* 1996;34:419–26. [https://doi.org/10.1016/0263-8223\(96\)00010-4](https://doi.org/10.1016/0263-8223(96)00010-4).
- [18] Kachanov L. Time of the rupture process under creep conditions. *Izvestia Akademii Nauk SSSR, Otdelenie Teekhnicheskikh Nauk* 1958;8:26–31.
- [19] Gudmundson P, Zang W. An analytic model for thermoelastic properties of composite laminates containing transverse matrix cracks. *Int J Solids Struct* 1993;30:3211–31. [https://doi.org/10.1016/0020-7683\(93\)90110-S](https://doi.org/10.1016/0020-7683(93)90110-S).
- [20] Li S, Wang M, Jeanmeure L, Sitnikova E, Yu F, Pan Q, et al. Damage related material constants in continuum damage mechanics for unidirectional composites with matrix cracks. *Int J Damage Mech* 2019;28:690–707. <https://doi.org/10.1177/1056789518783239>.
- [21] Li S, Reid SR, Soden PD. A continuum damage model for transverse matrix cracking in laminated fibre-reinforced composites. *Philos Trans Roy Soc Lond Ser A: Math Phys Eng Sci* 1998;356:2379–412. <https://doi.org/10.1098/rsta.1998.0278>.
- [22] Pagano NJ. Exact moduli of anisotropic laminates. In: Reddy J, editor. *Mech compos mater* Dordrecht: Springer; 1994. p. 210–31. https://doi.org/10.1007/978-94-017-2233-9_18.
- [23] Sun C, Li S. Three-dimensional effective elastic constants for thick laminates. *J Compos Mater* 1988;22:629–39. <https://doi.org/10.1177/002199838802200703>.
- [24] Tong J, Guild FJ, Ogin SL, Smith PA. On matrix crack growth in quasi-isotropic laminates – II. Finite element analysis. *Compos Sci Technol* 1997. [https://doi.org/10.1016/S0266-3538\(97\)00083-3](https://doi.org/10.1016/S0266-3538(97)00083-3).
- [25] Groves S, Harris C, Highsmith A, Allen D, Norvell R. An experimental and analytical treatment of matrix cracking in cross-ply laminates. *Exp Mech* 1987;27:73–9. <https://doi.org/10.1007/BF02318867>.
- [26] McCartney LN, Schoepner GA, Becker W. Comparison of models for transverse ply cracks in composite laminates. *Compos Sci Technol* 2000;60:2347–59. [https://doi.org/10.1016/S0266-3538\(00\)00030-0](https://doi.org/10.1016/S0266-3538(00)00030-0).
- [27] Berthelot J-M. Transverse cracking and delamination in cross-ply glass-fiber and carbon-fiber reinforced plastic laminates: Static and fatigue loading. *Appl Mech Rev* 2003;56:111–47. <https://doi.org/10.1115/1.1519557>.
- [28] Nairn JA, Hu S. The formation and effect of outer-ply microcracks in cross-ply laminates: a variational approach. *Eng Fract Mech* 1992;41:203–21. [https://doi.org/10.1016/0013-7944\(92\)90181-D](https://doi.org/10.1016/0013-7944(92)90181-D).
- [29] Li S, Reid SR, Soden PD. A finite strip analysis of cracked laminates. *Mech Mater* 1994;18:289–311. [https://doi.org/10.1016/0167-6636\(94\)90041-8](https://doi.org/10.1016/0167-6636(94)90041-8).
- [30] Li S, Hafeez F. Variation-based cracked laminate analysis revisited and fundamentally extended. *Int J Solids Struct* 2009;46:3505–15. <https://doi.org/10.1016/j.ijsolstr.2009.03.031>.
- [31] Johnson P, Chang FK. Characterization of matrix crack-induced laminate failure – Part I: Experiments. *J Compos Mater* 2001;35:2009–35. <https://doi.org/10.1106/7RN1-PFBN-XQR9-3KDK>.
- [32] Fikry M, Kitamura R, Ogihara S. Effect of matrix cracking on mechanical properties in FRP angle-ply laminates. M&M 2017 Zairyorikigaku conference The Japan Society of Mechanical Engineers Materials & Mechanics Division; 2017. p. 818–21. <https://doi.org/10.1299/jsmemm.2017.OS1014>.
- [33] Lundmark P, Varna J. Constitutive relationships for laminates with ply cracks in in-plane loading. *Int J Damage Mech* 2005;14:235–59. <https://doi.org/10.1177/1056789505050355>.
- [34] Lundmark P, Varna J. Crack face sliding effect on stiffness of laminates with ply cracks. *Compos Sci Technol* 2006;66:1444–54. <https://doi.org/10.1016/j.compscitech.2005.08.016>.
- [35] Varna J. Physical interpretation of parameters in synergistic continuum damage mechanics model for laminates. *Compos Sci Technol* 2008;68:2592–600. <https://doi.org/10.1016/j.compscitech.2008.04.037>.
- [36] Benthem J, Koiter WT. Asymptotic approximations to crack problems. In: Sih G, editor. *Mechanics of fracture 1: methods of analysis and solutions of crack problems* The Netherlands: Leyden; 1973. p. 131–78. https://doi.org/10.1007/978-94-017-2260-5_3.
- [37] Tada H, Paris P, Irwin G. *The stress analysis of cracks handbook*. 3rd ed. New York: The American Society of Mechanical Engineers; 2000. <https://doi.org/10.1115/1.801535>.
- [38] Tong J, Guild FJ, Ogin SL, Smith PA. On matrix crack growth in quasi-isotropic laminates-I. Experimental investigation. *Compos Sci Technol* 1997. [https://doi.org/10.1016/S0266-3538\(97\)00080-8](https://doi.org/10.1016/S0266-3538(97)00080-8).
- [39] Pagano N, Schoepner G, Kim R, Abrams F. Steady-state cracking and edge effects in thermo-mechanical transverse cracking of cross-ply laminates. *Compos Sci Technol* 1998;58:1811–25. [https://doi.org/10.1016/S0266-3538\(98\)00047-5](https://doi.org/10.1016/S0266-3538(98)00047-5).
- [40] Dvorak G, Laws N. Analysis of first ply failure in composite laminates. *Eng Fract Mech* 1986;25:763–70. [https://doi.org/10.1016/0013-7944\(86\)90039-1](https://doi.org/10.1016/0013-7944(86)90039-1).
- [41] McCartney LN, Schoepner GA. Predicting the effect of non-uniform ply cracking on the thermoelastic properties of cross-ply laminates. *Compos Sci Technol* 2002;62:1841–56. [https://doi.org/10.1016/S0266-3538\(02\)00091-X](https://doi.org/10.1016/S0266-3538(02)00091-X).
- [42] Schoepner GA, Pagano NJ. Stress fields and energy release rates in cross-ply laminates. *Int J Solids Struct* 1998;35:1025–55. [https://doi.org/10.1016/S0020-7683\(97\)00107-8](https://doi.org/10.1016/S0020-7683(97)00107-8).